Strength and Failure Characteristics of SMC-R Composites under Biaxial Loads

by

Monish Urapakam Ramakrishnan

**A thesis submitted in partial fulfilment
of the requirements for the degree of
Master of Science in Engineering
(Automotive Systems Engineering)
in the University of Michigan – Dearborn
2017**

Master's Thesis Committee:

> **Professor Pankaj K. Mallick, Chair
> Professor HongTae Kang
> Raghuram Mandapati, Tenneco Automotive Operating Company Inc.**

To my Parents

ACKNOWLEDGMENTS

TABLE OF CONTENTS

CHAPTER 4: FATIGUE BEHAVIOR OF CARBON FIBER SMC-R IN BIAXIAL LOADING

CHAPTER 5: CONCLUSIONS

REFERENCES

LIST OF FIGURES

LIST OF TABLES

ABSTRACT

Sheet molding compound composites containing randomly oriented short fibers (SMC-R) are among the most commonly used composites in the automotive and many non-aerospace applications. They are also finding a few niche applications in the aerospace industry. Many studies have reported on static and fatigue properties of SMC-R composites under uniaxial loading conditions. However, there are many applications in which they may be subjected to biaxial loads and their biaxial properties have not been reported in the literature.

This study considers the strength and failure characteristics of SMC-R under biaxial loading conditions that were generated using various combinations of normal and shear stresses ranging from uniaxial tension to shear. Glass fiber and Carbon fiber SMC-R were the materials used for quasi-static tests and carbon fiber SMC-R was used for fatigue tests. In addition to determining the strength properties, this study also includes damage development process and failure prediction under biaxial loading. Finite Element Analysis was used to understand and verify the stress distribution in the specimen.

It was observed that the presence of shear stress decreases the tensile stress at failure for both glass and carbon fiber SMC-R. Depending on the stress biaxiality ratio, macroscopic damage development in both materials was initiated at 95 to 99% of the peak load. For both materials, a knee load was observed above which the material behaved non-linearly. Finite element analysis confirmed the damage development location in quasi-static tests. The biaxial failure load prediction seems to follow Hill's anisotropic yield criterion. The carbon fiber SMC-R exhibited a high degree of scatter in both quasi-static strength and fatigue life. Weibull analysis was performed to determine its strength characteristics of this material.

CHAPTER 1

INTRODUCTION

This chapter introduces the study being conducted, background information regarding sheet molding compounds, biaxial loading, and failure prediction, and the objectives of this research.

1.1 Introduction

Increasingly stringent pollution control regulations, fuel efficiency guidelines and customer expectations have propelled the automotive industry to develop innovative solutions to improve vehicle efficiency. Vehicle weight reduction plays a major part in meeting the efficiency targets. Among various strategies for vehicle weight reduction, one key strategy is to substitute currently used materials with more lightweight alternative, such as fiber reinforced polymer composites.

Composite materials have the advantage of high strength and stiffness compared to conventional materials such as steel, per unit mass. One great advantage of composites is that they allow for variation in constituents and their configurations to tailor the properties meet the design and performance requirements of structures and components in consideration. All these factors combined make it a very attractive lightweight substitute for conventional materials. The use of composites in a car has as a result, spread from exterior and interior body panels to engine components. Fiber reinforced polymers (FRP) form a major portion of the composites used in the automotive industry. FRP is being used in exterior body parts such as door panels, bumpers, hood etc. due to their high stiffness and low cost. Certain engine components such as timing belt cover, intake manifolds are made of glass fiber reinforced polymers to help reduce weight and complexity in component assembly. However, the use of

FRP in BIW or for any structural application was limited to high performance cars due to prohibitive cost and low production rates. Recent advances in fiber and matrix technology, allowing for better mechanical properties and faster production rates have made them an attractive choice for BIW components such as A-pillar, B-pillar, sills, transmission tunnel, et.al.

The increase in the use of composites has prompted a large amount of research to be conducted on understanding the behavior of composites under various loading conditions. The properties of continuous fiber and discontinuous fiber under uniaxial quasi static and cyclic load are well documented [1-5]. A large amount of research has also gone in to the behavior of continuous fiber composites under biaxial load due its anisotropic nature [6-9]. There is, however, no research on the behavior of randomly oriented short fiber composites under biaxial load. Therefore, the aim of this research is to understand the strength and failure of short fiber composites under different biaxial load cases. The modified Arcan test method [10] was used to conduct the experiments.

1.2 Sheet Molding Compound

Many body and engine components which use FRP are made of sheet molding compounds (SMC). Apart from being a lightweight alternative, SMC also show good dent resistance, help reduce assembly costs through part integration, and have significantly lower tooling costs when compared with steel. Also, SMC offers component designers with flexibility by accommodating complex shapes and depth of draw range.

SMC are thin sheets of fiber reinforced polymer composites which are manufactured by distributing fibers between two thin layers of a thermoset resin such as polyesters, vinyl esters or an epoxy. The thin sheets are stored in the form of rolls and are compression molded to the desired shape in a heated matched-metal mold and under high pressure.

Many types of SMC currently being used can be classified based on fiber length and orientation such as, SMC-R, containing random fiber orientation and discontinuous fibers having length much greater than its thickness; SMC-CR, containing alternating layers of unidirectional continuous and randomly oriented discontinuous fibers; and XMC, containing continuous fibers laid out in an X pattern and discontinuous fibers dispersed in the matrix [11]. SMC, SMC-CR and

XMC have excellent strength and stiffness in the direction of fiber orientation, but poor mechanical properties perpendicular to fiber orientation, making them suitable for highly specialized components only.

SMC-R on the other hand is planar isotropic and has a better stiffness to weight and strength to weight ratios compared to steel. Having randomly orientated discontinuous fibers, manufacturing of SMC-R saves a lot of time in the pre-compounding of fibers in the thermoset resin matrix resulting in higher production volumes and lower manufacturing costs, making it a favorite for many automotive and non-automotive application.

1.2.1 Manufacturing of SMC-R

A typical SMC is not composed of just a resin and fibers, additional materials are added to the resin to improve the properties. In general, the resin formulation contains resin paste, low shrink additive, filler, catalyst, thickener, and inhibitor.

Low shrink additives are added to reduce part shrinkage, when cooling from processing temperature to room temperature. It also helps eliminate defects such as surface waviness and improves surface finish. Catalyst is added to initiate the polymerization reaction at elevated temperatures in mold cavity. Thickener is used to increase the viscosity of the SMC sheets to a high enough value storage, so that it is hard enough to be cut into the desired shape before molding. The effects of the thickener are negated when the SMC sheets are placed in the mold and heated. The purpose of the inhibitor is to prevent the resin from curing before the compression molding process. Other additives such as pigments may be added to get the desired color in the resin paste.

The manufacturing of SMC-R is divided into two phases. The first phase involves the production of composite sheets and the second phase, is the molding of composite sheets to desired shape. Figure 1.1 shows the first stage of SMC-R production. In this process, long strands of fiber are chopped to the desired length and spread uniformly over a thin layer of resin. Care is taken to ensure that the chopped fiber orientation is random. After this, another layer of resin is laid on top of this and the sandwich is passed through a series of compacting rollers. These rollers ensure that the two layers of resin and the fibers bond together, it also

3
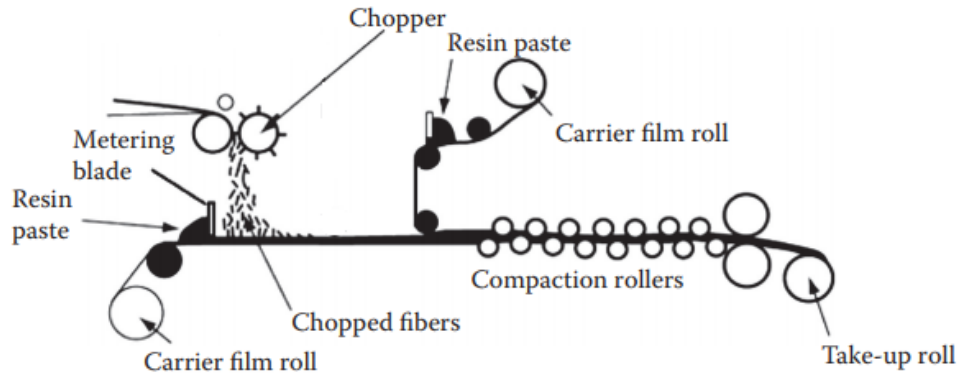
Figure 1.1 Production of SMC-R sheet

helps to reduce the thickness to the desired extent. This continuous sheet of SMC-R is rolled up and stored for further processing.

The compression molding process is used to convert the SMC-R sheets to the desired shape and size, and cure the resin in the material. Figure 1.2 gives a schematic representation of the compression molding process. The different steps involved in the process are as follows, first the required number of SMC-R sheets are cut to size and stacked which is called as charge.
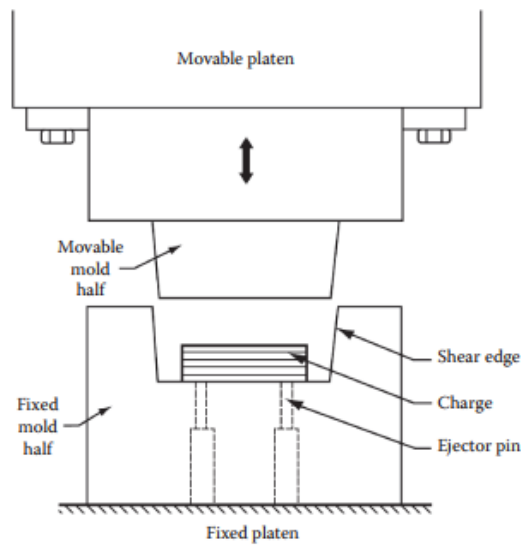
Figure 1.2 Compression molding of SMC-R

The charge is then placed in the mold cavity and the upper die is lowered quickly onto the charge. Once, the upper die comes in contact with the charge, it is lowered at a much slower rate to a pre-set pressure level. The mold surface is heated, which lowers the viscosity of the resin. The composite flows easily and spreads across the cavity. The pressure on the charge also helps remove any entrapped air and avoids cavity formation.

The mold is kept closed for an extended period of time even after complete filling to cure the thermoset matrix thoroughly. Depending on size of part and thickness the cure time may vary from 1 minute to several minutes. After the desired level of cure is achieved, the mold is opened, part is taken out and cooled at room temperature. The component may require additional finishing operations such as edge trimming, hole drilling etc.

1.2.2 Fiber Orientation in SMC-R

A major advantage of SMC-R composites is its planar isotropic behavior, which is achieved as the discontinuous fibers in random orientation are incorporated into the matrix. However, during the processing of the SMC-R charge to the finished product, the thickened resin transforms into viscous fluid and flows outwards in the mold cavity. During this step, the fibers move along with the resin resulting in a change in fiber orientation and distribution. This may result in the fiber orientation not being completely random. A large amount of research has been conducted to analyze the effect of manufacturing parameters on the fiber orientation and resin flow.

Any variation in the thickness of the part being molded also affects the flow of resin and hence, the orientation of fibers. A change in section thickness from a thicker to a thinner section results in a convergent flow and fiber orientation in one direction. If the opposite occurs, the divergent flow randomizes the fiber orientation. Any change in the part shape or size affects the flow of resin and hence fiber orientation. This could be caused due to holes, inserts, ribs etc. Thickness of the charge and mold closing speeds affect the uniform distribution of the charge [12]. At high closing speeds, thickness does not affect the flow and charge extends outwards uniformly, with slip between die surface and charge surface. At slow closing speeds, thickness of the charge plays a key role. In thick charges, there is decrease in viscosity from outer layer to inner layer of the charge, this causes a difference in flow between each layer, with the outer layers spreading out more.
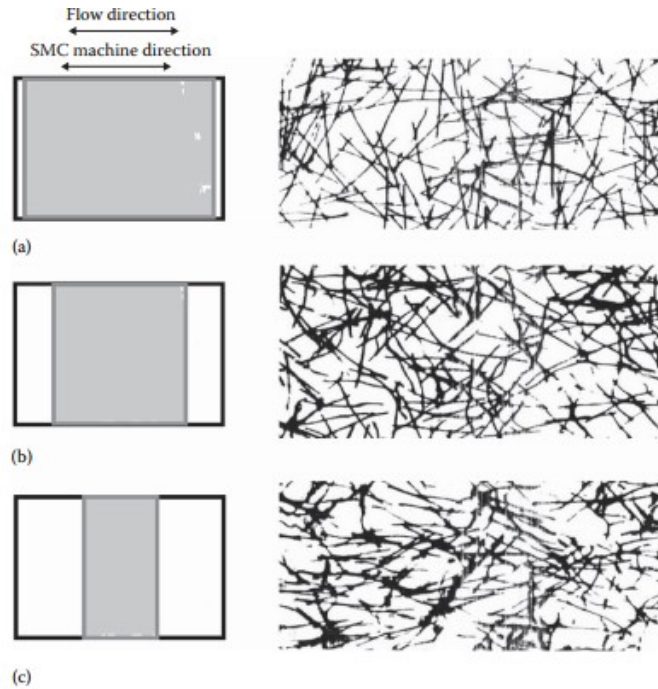
Figure 1.3: Effect of charge location and size on the fiber orientation. [11]

The size of the charge affects the fiber orientation in SMC-R [11]. Figure 1.3 illustrates this phenomenon. A lower mold coverage results in a larger area for the resin to flow and as a result a large portion of the fibers are oriented in resin flow direction. And, if the charge is placed as shown in Figure 1.3 (c), the composite is seen to be anisotropic as the strength is much greater in the direction of resin flow.
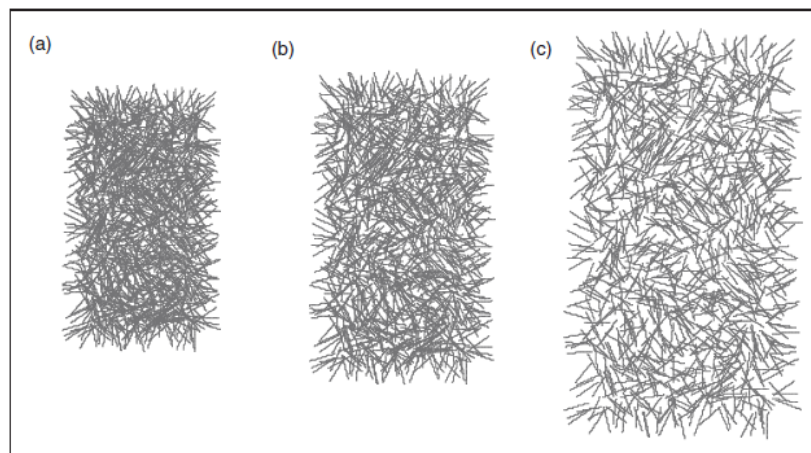
Figure 1.4: Simulation of fiber distribution in biaxial flow. [13]

If the flow of resin is biaxial, then there is negligible effect on the randomness of fiber orientation despite the resin flow [13] as shown in Figure 1.4. Therefore, it can be concluded that, irrespective of the charge size, if the flow of resin is uniform in all directions under pressure, the planar isotropic behavior can be maintained.

1.2.3 Mechanical Characteristics of SMC-R

Due to the random orientation and distribution of chopped fibers in SMC-R, the properties are assumed to be the same in all directions in the plane, i.e. it is planar isotropic. However, due to the heterogeneous nature of the material and flow induced anisotropy during manufacturing, different sections of the same compression molded SMC-R part may show variations in the properties [1,11-13]. Therefore, since the inception of SMC in 1960's extensive research has been conducted to study and characterize the mechanical properties of SMC-R in uniaxial monotonic and cyclic conditions.

A comprehensive study conducted by Denton [1] on SMC-R50 shows the behavior under different uniaxial load conditions. It is seen that strength of SMC-R under shear stress is low compared to its tensile and flexural strength. Under tensile load, the relationship between stress and strain is initially linear followed by a non-linear relationship till failure. The point of transition from linear to non-linear curve is referred to as the knee point [14]. Previous research by Watanabe and Yasuda [15] showed that craze marks developed at the knee point, these craze marks are due to damage development in the matrix. Also, the study shows that an increase in fiber volume fraction leads an increase in the tensile modulus and strength, but the knee point shows minor change.

The heterogeneous nature of the composite and degradation of strength in polymers under cyclic load makes the study of SMC-R under cyclic load important. Under Tensile fatigue loading, SMC-R shows a similar degradation in stiffness. This change in stiffness is due to the evolution of microscopic damage in the material [16] caused by matrix cracking, fiber-matrix debonding and fiber-end cracking. Also, due to the randomly dispersed fibers SMC-R, the fatigue life at each load level is known to vary within a batch and across different batches. Due to the scatter in fatigue life data, the fatigue life is expressed in terms of probability of failure at each stress level using a Weibull distribution or a lognormal distribution. Empirical relations such as Coffin and Manson's

relation and Basquin's relation have been used to predict fatigue life, showing good correlation with test data [17].

1.3 Biaxial Loading

Multiaxial loading on a material occurs when two or more types of stresses act on the material simultaneously. In this research, biaxial loading on the specimen induces normal and shear stresses. For, thin laminates of SMC-R we will consider only the plane stress condition. In which stresses acting on the laminate are σ_{xx}, σ_{yy} and τ_{xy} as shown in figure 1.5.

The principal normal stresses, σ_1 and σ_2, on the laminate can be calculated in terms of σ_{xx}, σ_{yy} and τ_{xy} using the following equations.

$$\sigma_1 = \frac{\sigma_{xx} + \sigma_{yy}}{2} + \sqrt{\left(\frac{\sigma_{xx} - \sigma_{yy}}{2}\right)^2 + \tau_{xy}^2}$$

$$\sigma_2 = \frac{\sigma_{xx} + \sigma_{yy}}{2} - \sqrt{\left(\frac{\sigma_{xx} - \sigma_{yy}}{2}\right)^2 + \tau_{xy}^2}$$

Different test methods have been used to determine the influence of static and fatigue biaxial loads on composites. This section will review commonly used test methods for composites and discuss the merits and demerits of each method.
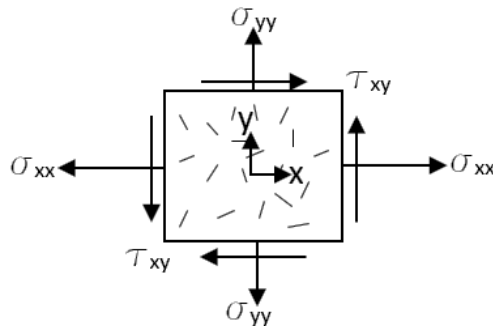
Figure 1.5: Stresses acting on a thin SMC-R laminate under plane stress condition.
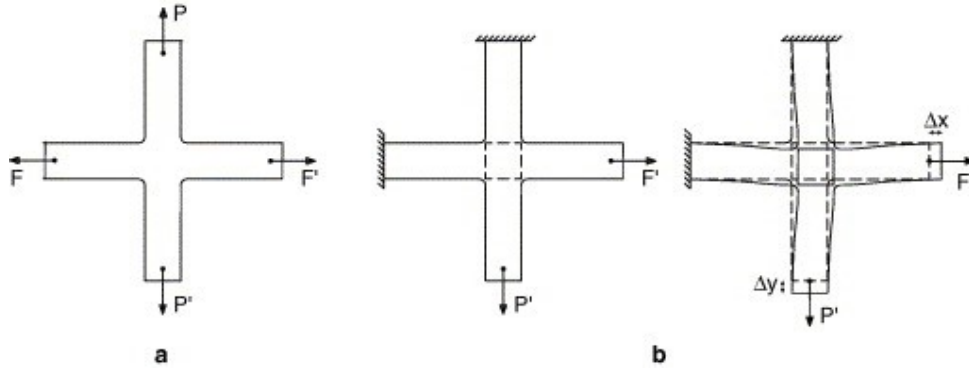
Figure 1.6: Cruciform Specimen Test method with (a) 4 actuators, (b) 2 actuators. [16]

1.3.1 Cruciform Specimen

Figure 1.2 shows a schematic of the cruciform specimen test method to obtain a biaxial stress zone at the critical section. In this test method, the load on each arm of the specimen is controlled to generate a biaxial load at the critical section, which is at the intersection of the two arms [19-21]. Recent study done by Smit et al. [19] developed a cruciform test method with four actuators (Figure 1.2 (b)) and digital image correlation to measure strain. This study used a specimen with lower thickness at the critical section notch fillets to ensure failure does not take place in the arms.

Cruciform specimen test method develops uniform biaxial stress field at the critical section, however, this test cannot be used to determine shear strength of the specimen. Also, the equipment used for testing is complex and expensive, and the design of the specimen makes it complex to manufacture.

1.3.2 Tubular Specimens

Test method developed with tubular specimen are versatile with the possibility of inducing different forms of biaxial stress. In this test, the thin tubular specimens are subjected to a combination of internal pressure, torsion and tensile or compressive stresses [22,23]. Figure 1.3 shows the test setup with a tubular specimen. Smith and Swanson [22] conducted extensive research on biaxial properties of various composites using this method due to the advantages this method offers such as, absence of free edges and ability to mimic the exact load conditions for various industrial applications.

There are however, several demerits to this test method. The results of this method cannot be compared to the properties of a composite sheets, specimen thickness affects the stress distribution through the walls, fabrication of specimen to ensure perfect tubular shape and alignment of specimen with test rig axis is difficult. Also, the entire test setup is expensive and complex.
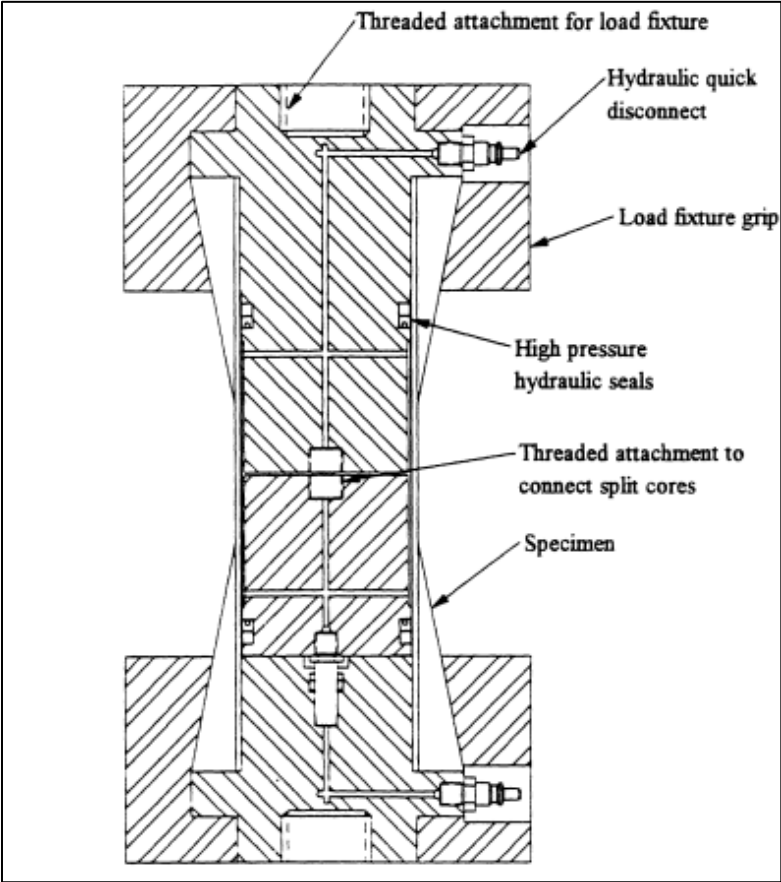
Figure 1.7: Biaxial test apparatus. [19]
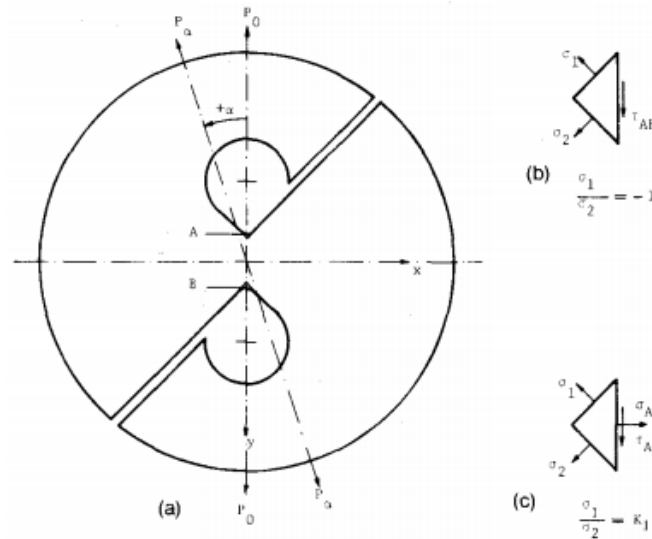
Figure 1.8: Arcan specimen and biaxiality ratios. [10]

1.3.3 Arcan Specimen

The Arcan specimen shown in Figure 1.8 was developed by Arcan et. al. [10] to study the in-plane characteristics of composite laminae under biaxial load. A combination of tensile or compressive and shear load can be applied to the specimen in this test and the biaxiality ratio can be varied by changing the orientation of the critical section with respect to the loading axis.

This test method can be carried out on a regular uniaxial test machine and eliminates the use of expensive equipment. Also, a uniform stress field is developed in the critical section of the specimen.

1.4 Research Objective

The objective of this research is to study the strength and failure characteristics of sheet molding compounds under biaxial load. Sheet molding compounds with randomly oriented discontinuous fibers show variations in properties due to heterogeneous nature of composite mixture and resin flow generated anisotropy during compression molding. Therefore, it is important to study the failure characteristics of the composite under different biaxial load conditions and determine their failure envelope. Lack of previous research in this area has prompted this study. The study takes into consideration quasi static as well as fatigue load conditions.

11

1.5 Thesis Outline

Behavior of SMC-R composites under biaxial load is studied in this thesis using modified Arcan test method. Carbon fiber and glass fiber SMC-R composites are the materials used in this study. The outline of the study is as follows:

1. Strength and failure characteristics of glass fiber SMC-R under biaxial load.

2. Strength and failure characteristics of carbon fiber SMC-R under biaxial load.

3. Finite element analysis of the stress distribution in Arcan Specimen.

4. Characteristics of carbon fiber SMC-R under biaxial fatigue load.

CHAPTER 2

STATIC BEHAVIOR OF GLASS FIBER SMC-R IN BIAXIAL LOADING

In this chapter, the test results of the glass fiber SMC-R specimens under quasi-static biaxial loads are presented. It includes a description of the damage development process and discusses the interaction of normal and shear stresses on the failure envelope. It also considers two failure prediction models and their applicability to glass fiber SMC-R composites.

2.1 Introduction

Extensive research has been done on the behavior of SMC-R composites under uniaxial monotonic and cyclic loads [1-5]. However, there is a lack of research on the performance of SMC-R under combined loading conditions in which both tensile and shear stresses are acting simultaneously on the material. This study considers the strength and failure characteristics of E-glass fiber SMC-R composite under biaxial loading conditions and the effect of shear stress on the tensile load carrying capacity of the material.

Previous work on strength behavior of composites under biaxial loading conditions have concentrated on continuous fiber-reinforced composites. There are different methods to perform biaxial tests as discussed in Chapter1. Cruciform specimen and tubular specimen are some of the commonly used biaxial test methods. However, these methods require complicated test setup. And, manufacturing of specimen is complex and difficult to get uniformity across all specimens. The Arcan test method is found to generate a nearly uniform biaxial stress across the critical section of the specimen and can be setup on existing uniaxial testing machines, eliminating costly test setups for biaxial experiments.
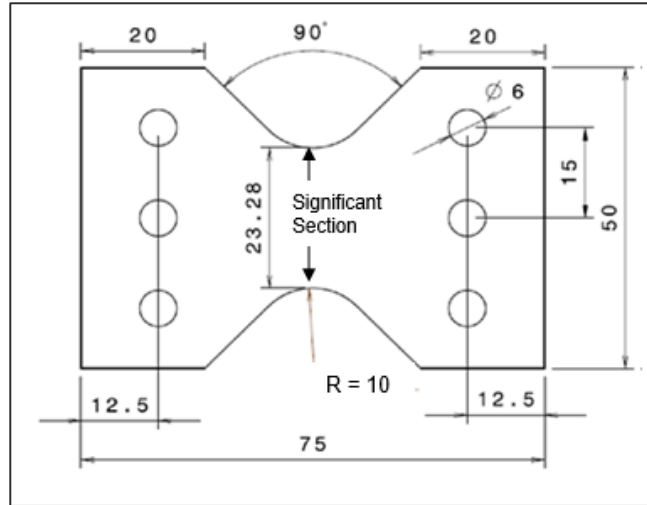
Figure 2.1: Butterfly-shaped Arcan specimen (dimensions are in mm)

In this study, the modified Arcan specimen that was originally developed by Arcan et al. [10] is used to biaxial behavior of composites. Recent work by Mandapati and Mallick [9] on biaxial fatigue behavior of fiber reinforced polymer laminates used a modified Arcan test method using butterfly-shaped Arcan specimens. Their test method was adopted for the current study.

2.2 Material

The specimens were machined from a compression molded flat plate of SMC-R65, which is a sheet molding compound composite containing 65 wt.% E-glass fibers in a vinyl ester matrix. The glass fibers are 25 mm long and randomly oriented in the x-y plane of the plate. Because of the random orientation of the fibers, the material is assumed to be planar isotropic, so that its modulus as well as strength are the same in all directions in its plane.

2.3 Specimen

A butterfly-shaped Arcan specimen is used for testing in uniaxial tension, shear and combined tension and shear modes. As shown in Figure 2.1, the overall external dimensions

Figure 2.2: Template used to machine specimens.

of the specimen are 75 mm x 50 mm x 2.9 mm. The 6-mm diameter holes on the specimen are used for clamping it to the test fixture shown in Figure 2.1. The notch angle is 90°. The width of the significant section between the 10-mm radius notches is 23.28 mm, so that the nominal significant area is 67.51 mm^2. The notch radius and notch angle were selected using a finite element study to provide a uniform stress distribution over 90% of the significant length. [25]

A template shown in Figure 2.2 was used to machine the Arcan specimens from compression molded flat plates. A diamond-shaped carbide-tipped router was used to machine the specimens on a high-speed routing machine. The template also served as guides to drill the 6 mm holes into the specimen. The machined specimen is shown in Figure 2.3. Before testing, the machined edges were smoothened using 240 and 400 grit sand papers.

Figure 2.3: Butterfly shaped Arcan specimen

2.4 Test Procedure

The monotonic tests were conducted on an MTS 810 servo-hydraulic testing machine with a tensile load capacity of 100 kN. The loading fixture, shown in Figure 2.4, was used to perform both uniaxial and bi-axial tests. The loading fixture is circular in shape with two sets of front and back plates. The plates contain holes every 15° apart along the circumference. The loading fixture was connected to the upper and lower jaws of the MTS machine using a three-pin arrangement at each end. The specimen was mounted between the front and back plates with three sets of M6 bolts and nuts with a clamping torque of 15 N.m.

The specimen orientation with respect to the loading direction, denoted by angle α in Figure 2.4, was varied to generate different combinations of tensile and shear stresses in the critical section of the specimens. The loading of the specimens was displacement controlled at 2 mm/min. Each test was continued until the load on the specimen was reduced to 10% of the peak load. Load and displacement data were acquired at a frequency of 100 Hz. A high definition camera was used to capture the damage development in the specimen and a high intensity CFL bulb was used to improve the visibility of damage development.
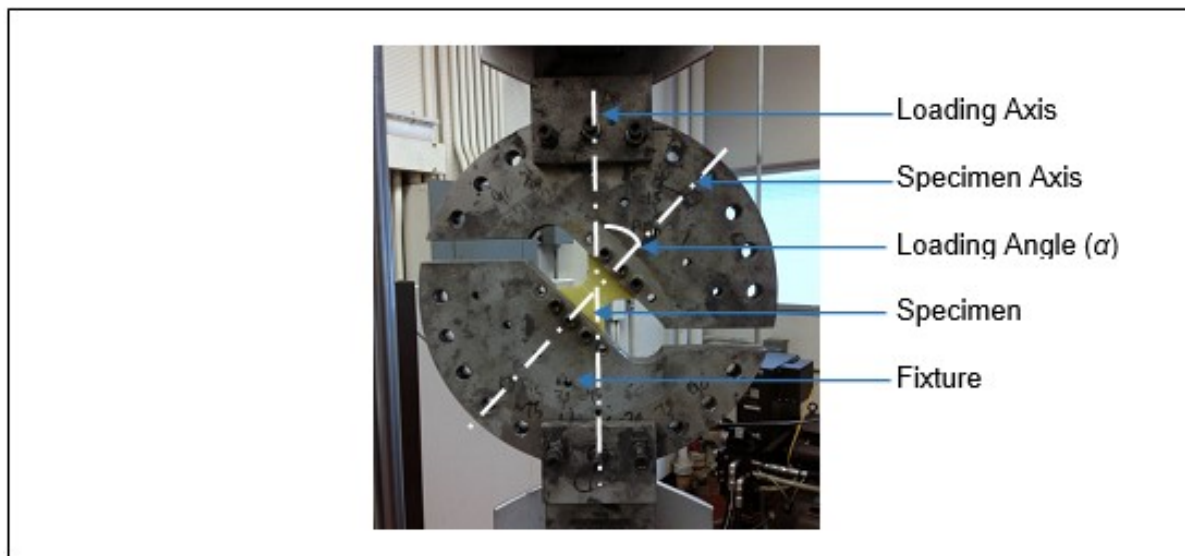
Figure 2.4: Arcan specimen mounted in the fixture.
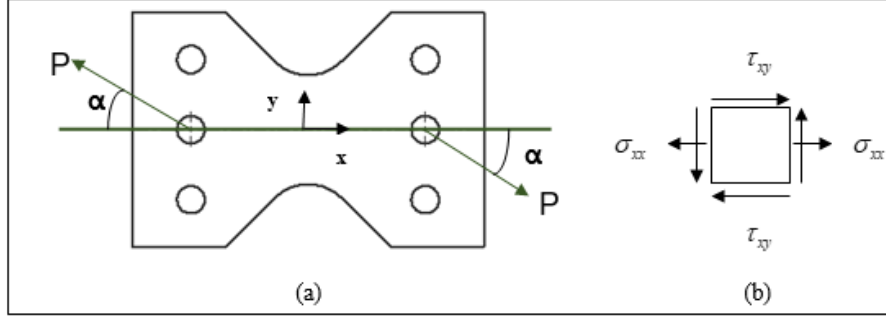
Figure 2.5: (a) Load P acting at angle α on the specimen (b) Normal and shear stresses acting on a stress element in the center of the critical section

Figure 2.5 (a) shows the load P acting on the specimen at an angle α and Figure 2.5 (b) shows the normal stress σ_{xx} and shear stress τ_{xy} acting on a stress element in the critical section of the specimen. The force components in the x and y directions are,

$$F_x = F \cos \alpha$$
$$F_y = F \sin \alpha$$

(2.1)

The average stresses in the critical section of area A are as follows

$$\sigma_{xx} = \frac{F_x}{A} = \frac{F \cos \alpha}{A}, \sigma_{yy} = 0$$
$$\tau_{xy} = \frac{F_y}{A} = \frac{F \sin \alpha}{A}$$

(2.2)

The biaxiality ratios [15] are defined as:

$$\lambda_y = \frac{\sigma_{yy}}{\sigma_{xx}}$$

$$\lambda_{xy} = \frac{\tau_{xy}}{\sigma_{xx}}$$

2.5 Quasi-Static Test Results

The butterfly-shaped Arcan specimens were tested at different loading angles varying from 0 to 90° at 15° intervals. Three specimens were tested at each loading angle. The tests conducted at 0° induces a uniaxial tensile stress and at 90° induces pure shear stress at the center of the

significant section. The tests conducted at angles between 0º and 90º induce varying biaxial stresses on the specimen.

The peak loads recorded for each specimen and biaxiality ratios are shown in Table 2.1. The average load is seen to decrease with an increase in loading angle from 0º to 45º; thereafter, the average peak load has become stable and does not show any significant variation.

Figure 2.6 illustrates the load-displacement curves for the specimens at seven different loading angles. From Figure 2.6, we can observe that the peak load decreased significantly as the loading angle was increased from 0 to 45º, and then it increased as the loading angle was increased to 60, 75 and 90º. The decrease in peak load between 0 and 60º occurred as the shear stress component on the specimen increased. The lowest peak load was observed at the 45º loading angle. At 75 and 90º loading angles where the shear stress component is more dominant than the tensile stress component, the shear stress at the peak load tended to show a plateau and the effect of tensile stress appears to be relatively small.

It can be observed in Figure 2.6 that after an initial linear segment, the load-displacement diagrams became non-linear until the peak load was reached. The degree of non-linearity increased as the loading angle was increased. In general, the transition from linear to non-linear segments is considered to be due to the appearance of damage in one or more locations in the material. The non-linear segment of the load-displacement diagram was accompanied by slow damage growth until the peak load was reached.

Macroscopically, two distinct damage developments were observed on the SMC-R specimens as shown in Figure 2.7. At 0º loading angle, a single crack started at one of the notch roots in the critical section and propagated along the width. In the case of 15º loading angle, a single crack was also observed, but it was slightly offset from the notch root. However, at higher loading angles, in most of the specimens two cracks were observed slightly offset from the notch roots. They started at opposite sides of the critical section and propagated along the width of the specimen in an arc. The distance of crack origin from significant section increased with an increase in the loading angle. This is shown in table 2.2.

Table 2.1: Quasi-Static Test Results

Specimen No.	Loading Angle (deg)	Peak Load (kN)	Average Peak Load (kN)	Knee Load (kN)	Average Knee Load (kN)
SMCR-001-St	0	10.361		5.4	
SMCR-002-St	0	11.399	10.85	5.7	5.6
SMCR-003-St	0	10.777		5.7	
SMCR-151-St	15	8.92		5.1	
SMCR-152-St	15	8.54	8.91	3.6	4.8
SMCR-153-St	15	9.268		5.7	
SMCR-301-St	30	7.742		4.4	
SMCR-302-St	30	9.274	8.17	4.3	4.3
SMCR-303-St	30	7.497		4.1	
SMCR-451-St	45	7.117		3.3	
SMCR-452-St	45	6.747	7.06	3.8	3.8
SMCR-453-St	45	7.331		4.2	
SMCR-601-St	60	7.06		3.5	
SMCR-602-St	60	6.983	7.12	3.9	3.8
SMCR-603-St	60	7.317		4	
SMCR-751-St	75	7.618		3.45	
SMCR-752-St	75	7.623	7.03	3.5	3.3
SMCR-753-St	75	5.841		3	
SMCR-901-St	90	7.531		4.1	
SMCR-902-St	90	7.387	7.25	3	3.7
SMCR-903-St	90	6.84		4	
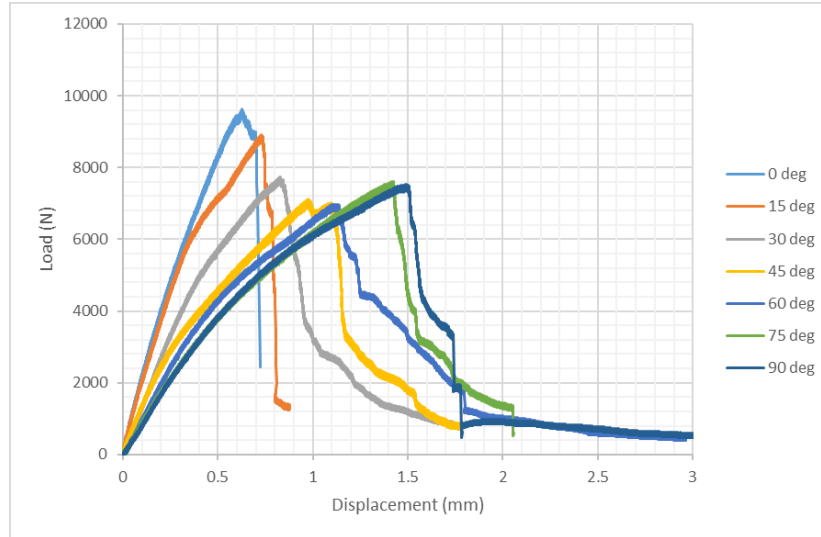
Figure 2.6: Load-displacement diagrams at different loading angles.

Table 2.2: Distance of Crack origin from Significant Section

Specimen No.	Distance from Significant Section
SMCR-001-St	0
SMCR-002-St	1.4
SMCR-003-St	0
SMCR-151-St	3.2
SMCR-152-St	4.6
SMCR-153-St	3.5
SMCR-301-St	4.7
SMCR-302-St	4.9
SMCR-303-St	3.9
SMCR-451-St	6.2
SMCR-452-St	7.9
SMCR-453-St	4.8
SMCR-601-St	8.4
SMCR-602-St	7
SMCR-603-St	6.5
SMCR-751-St	5.3
SMCR-752-St	5.1
SMCR-753-St	4.7
SMCR-901-St	8.1
SMCR-902-St	7.6
SMCR-903-St	8.4

20

Figure 2.7: Damage locations in specimens at 0° (left) and 45° (right) loading angles

As the loading angle is increased, the slope of the load vs displacement curve, i.e., stiffness of the material is observed to decrease. Also, the development of crack is observed to be slower at higher loading angles, compared to the pure tension case at 0° loading angle where there was an abrupt failure as soon as the peak load is reached. The failure occurring in the specimen under biaxial load is observed to be a form of cleavage. Crack initiation and growth occurs due to high tensile and shear stresses close to critical section.

Figures 2.8 to 2.14 show the damage development in the specimen under different loading angles. The series of four images of the specimen shows the progression of crack from initiation to specimen failure from top to bottom at the macroscopic level. The load and displacement at the point each image is taken is indicated in the graph on the left. Under quasi static loading, first cracks are heard along with splinters flying out close to the knee load. As, the damage progresses, macroscopic crack initiation is observed close to the peak load. As, the displacement increases, in pure tension case the crack propagates along the width of the critical section along with an abrupt decrease in the strength. Under biaxial or shear load the crack propagates in an arc starting near the critical section, the crack growth is accompanied by a gradual decrease in strength.
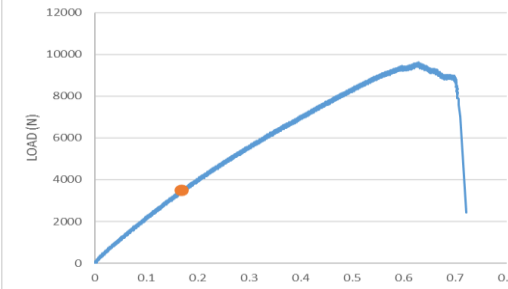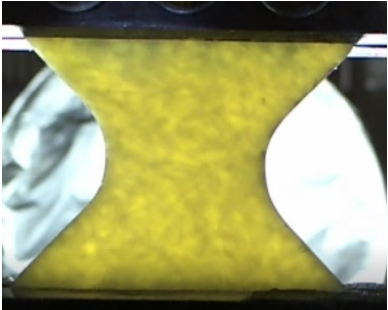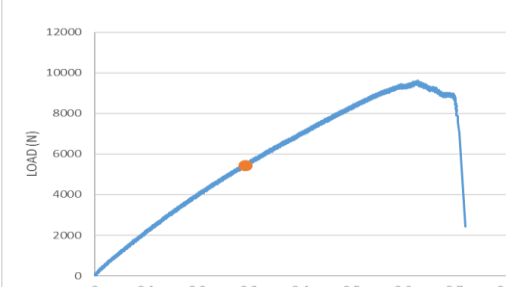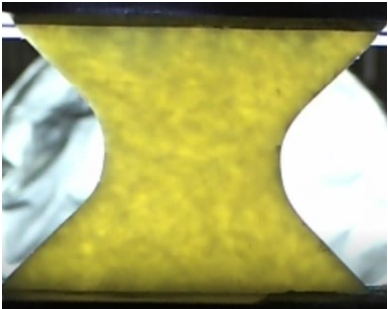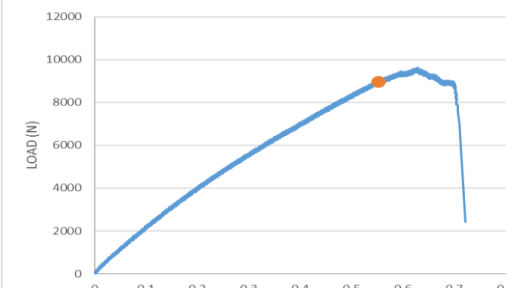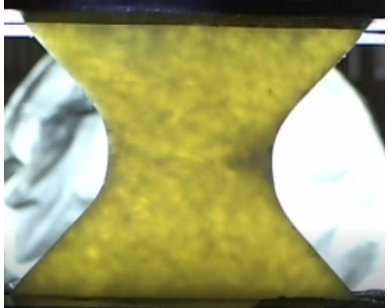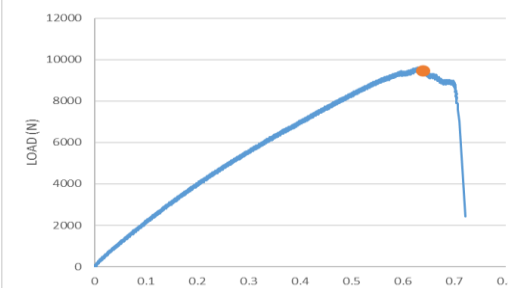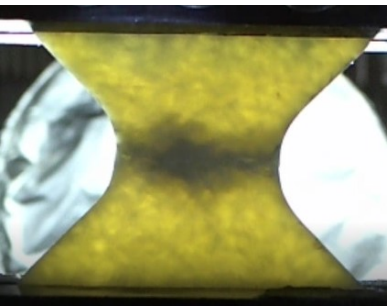
Time/ Displacement	Damage Development	
10.008 s/ 0.168 mm		
17.504 s/ 0.292 mm		
33.002/ 0.552 mm		
38.254 s/ 0.638 mm		

Figure 2.8: Damage development in Arcan specimen at 0º
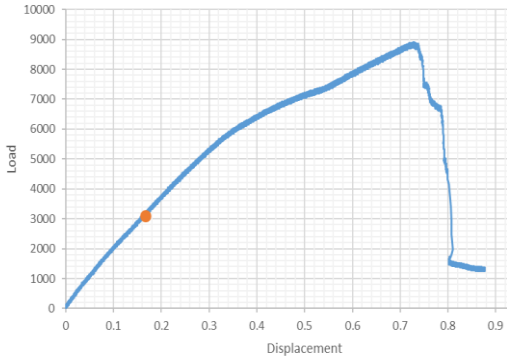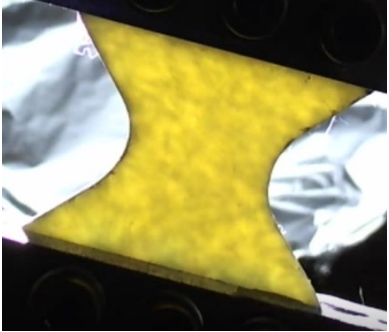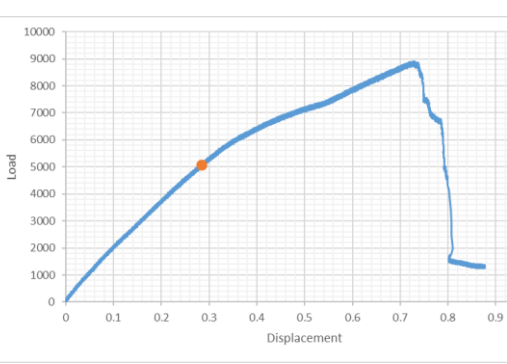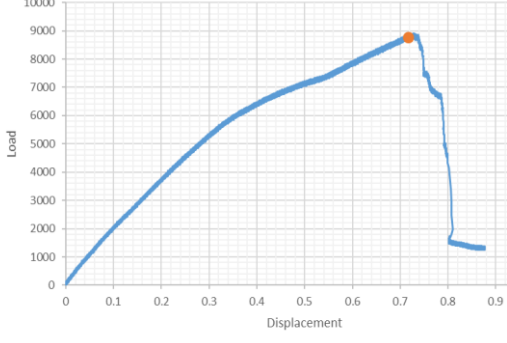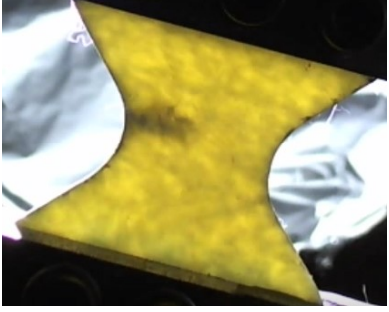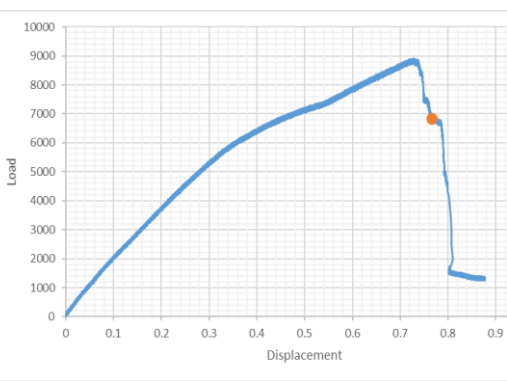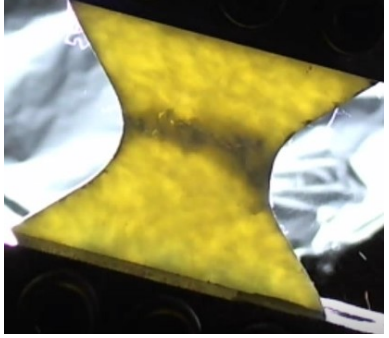
Time/ Displacement	Damage Development
10.005 s/ 0.166 mm	
17.004s/ 0.284 mm	
44.002 s/ 0.733 mm	
46.005 s/ 0.765	

Figure 2.9: Damage development in Arcan specimen at 15º

Time/ Displacement	Damage Development	
10.002 s/ 0.165 mm		
21.03 s/ 0.349 mm		
46.002 s/ 0.765 mm		
93.002 s/ 1.549 mm		
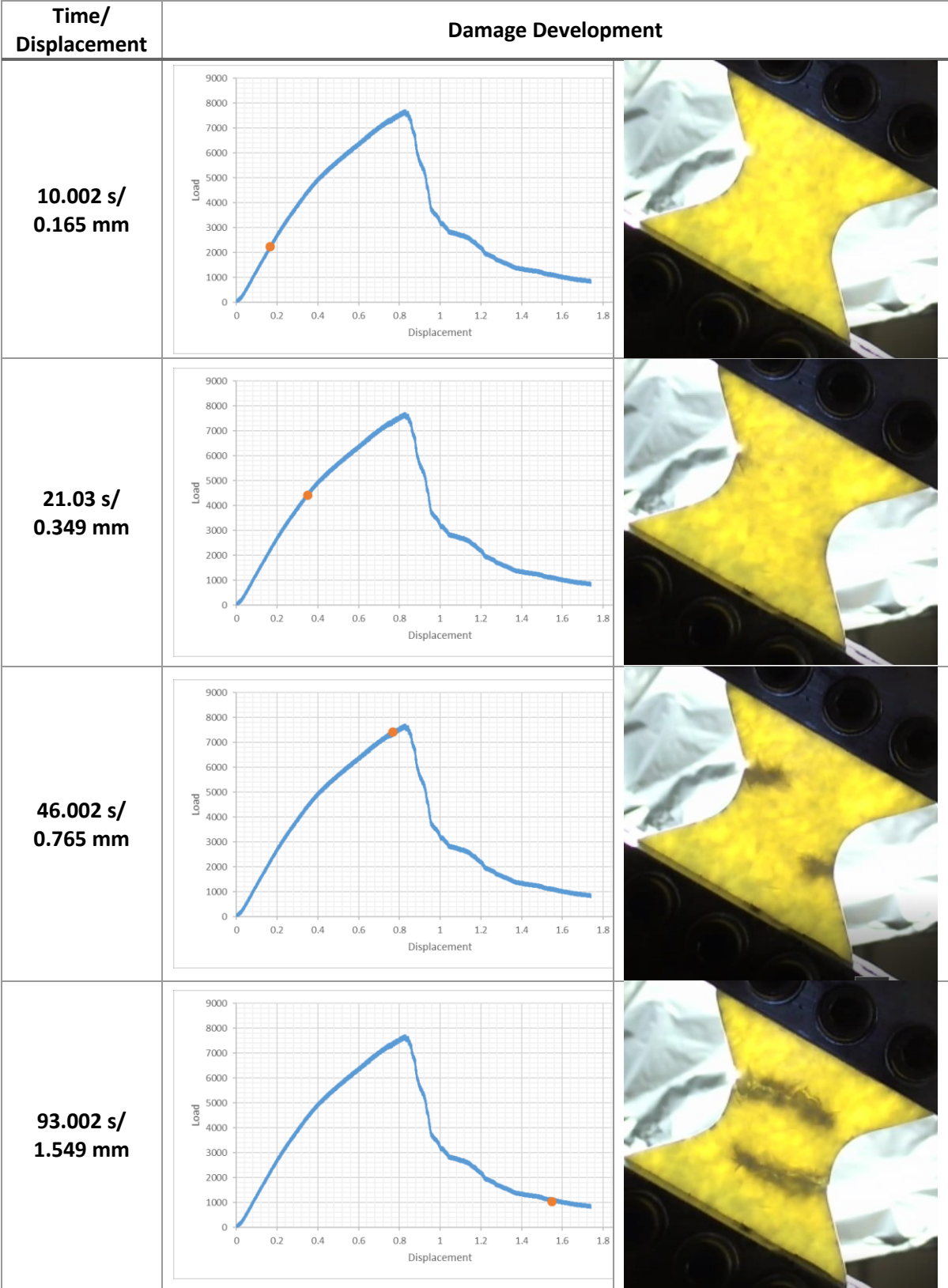
Figure 2.10: Damage development in Arcan specimen at 30º

Time/ Displacement	Damage Development	
10.005 s/ 0.166 mm		
18.007 s/ 0.299 mm		
65.002 s/ 1.081 mm		
87.009 s/ 1.449 mm		
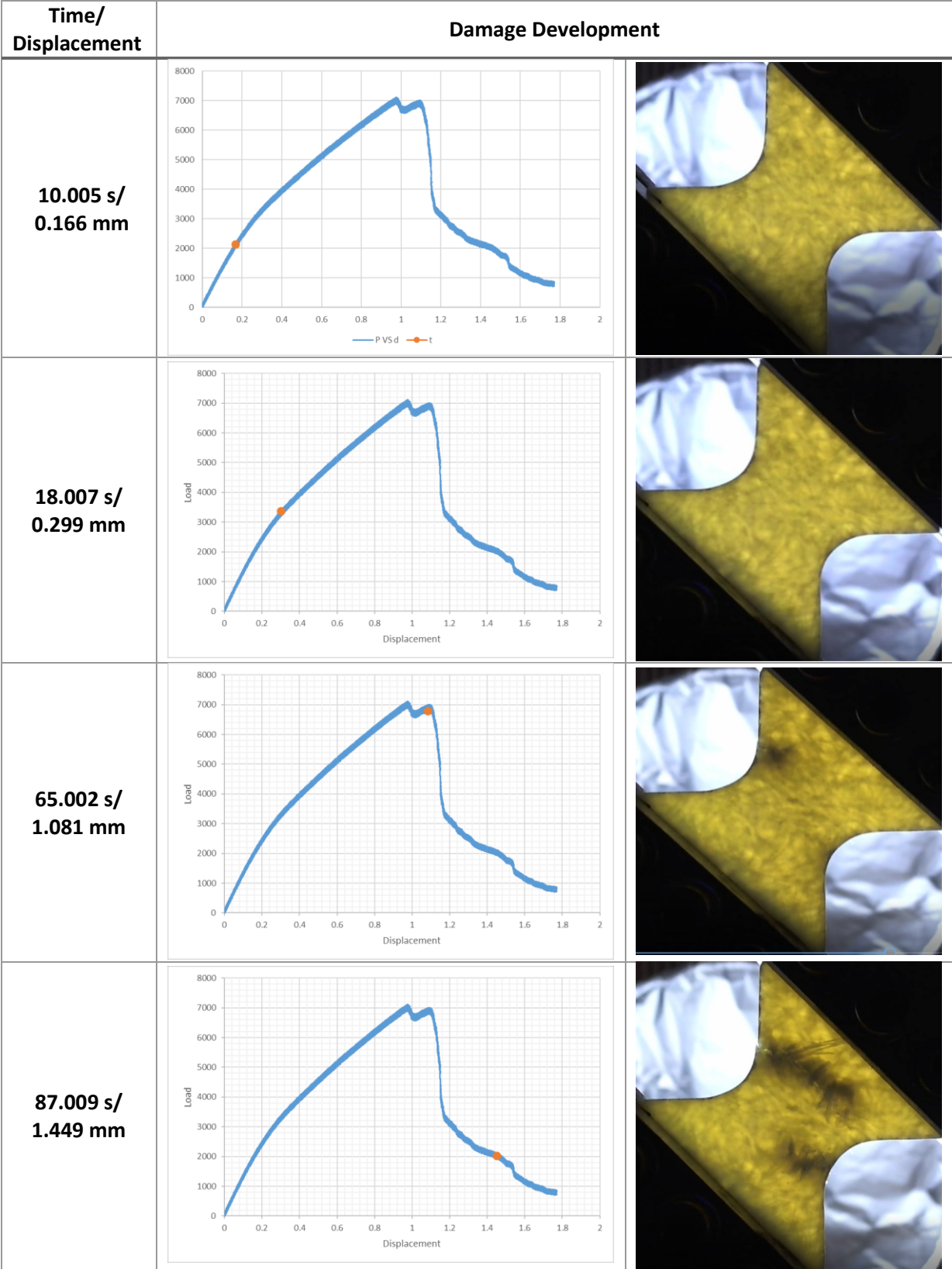
Figure 2.11: Damage development in Arcan specimen at 45º
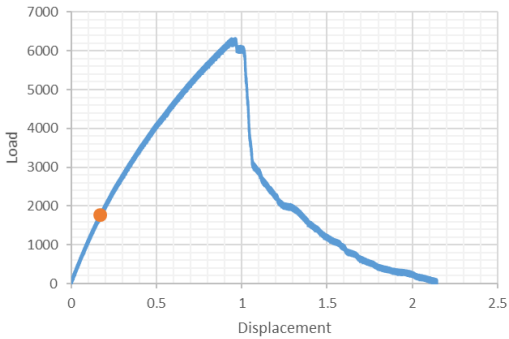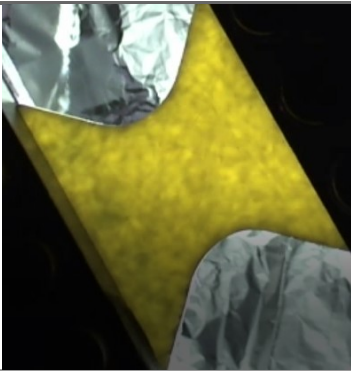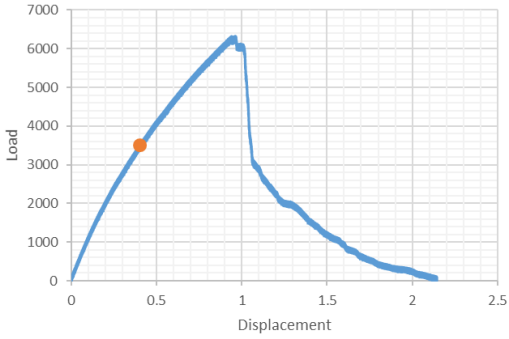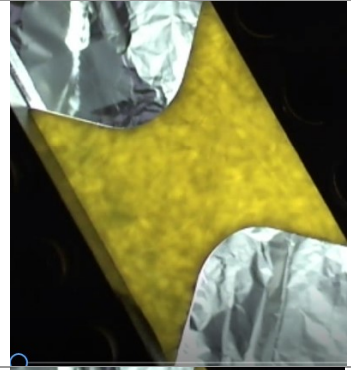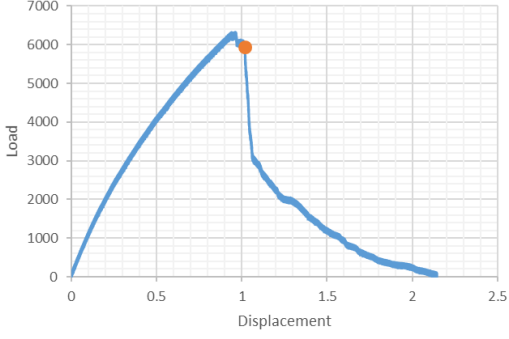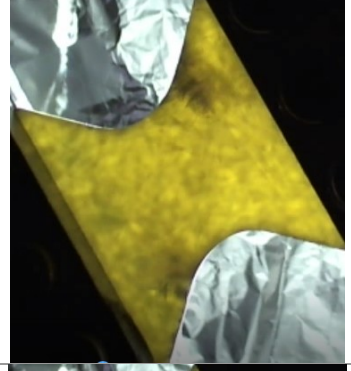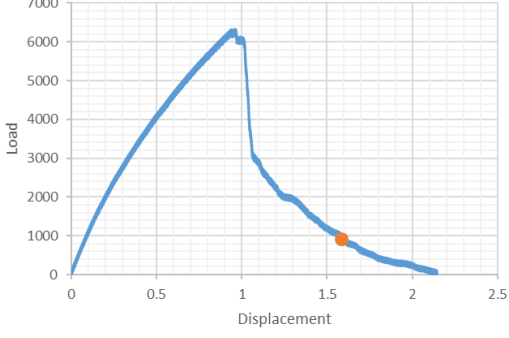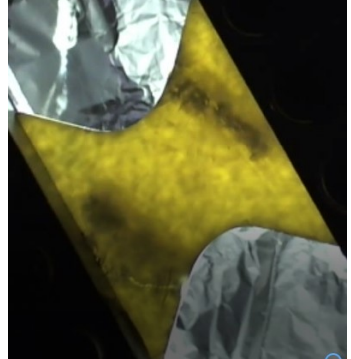
Time/ Displacement	Damage Development	
10.004 s/ 0.165 mm		
24.02s/ 0.398 mm		
61.009 s/ 1.015 mm		
95.009 s/ 1.582 mm		

Figure 2.12: Damage development in Arcan specimen at 60º
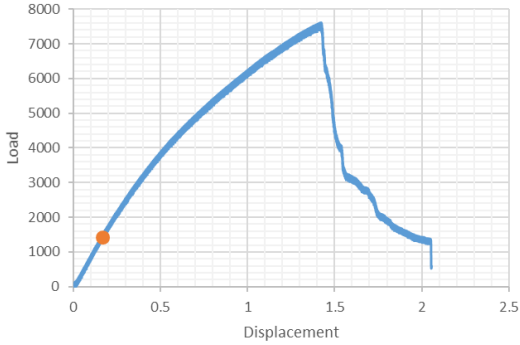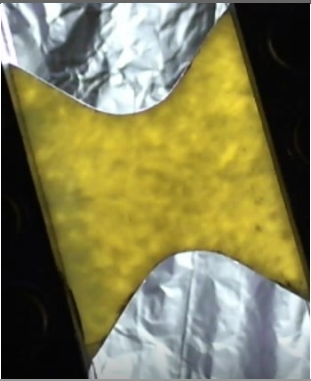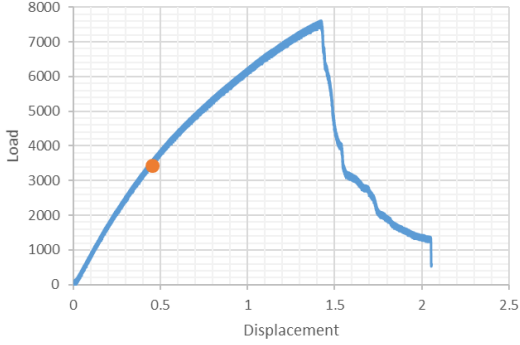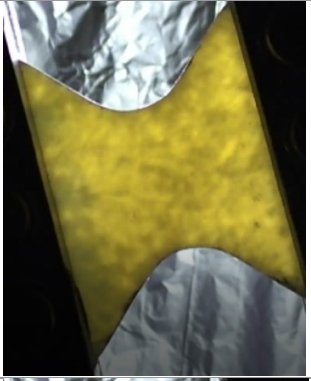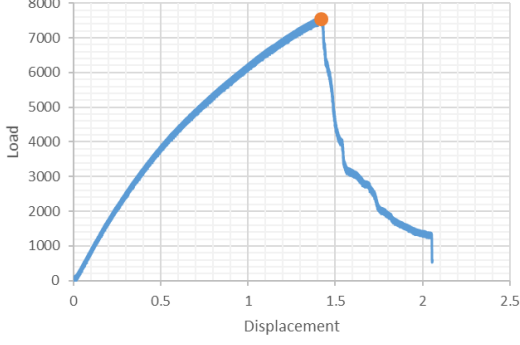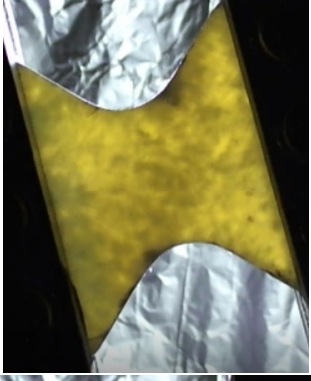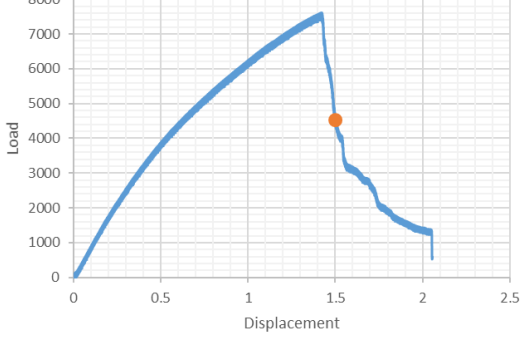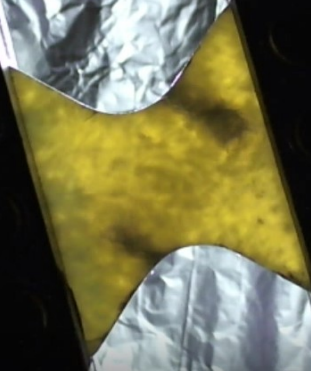
Time/ Displacement	Damage Development	
10.003 s/ 0.166 mm		
27.001 s/ 0.449 mm		
85.002 s/ 1.415 mm		
90.006 s/ 1.498 mm		

Figure 2.13: Damage development in Arcan specimen at 75º

Time/ Displacement	Damage Development	
10.008 s/ 0.166 mm		
33.002s/ 0.549 mm		
90.001 s/ 1.499 mm		
100.009 s/ 1.666 mm		
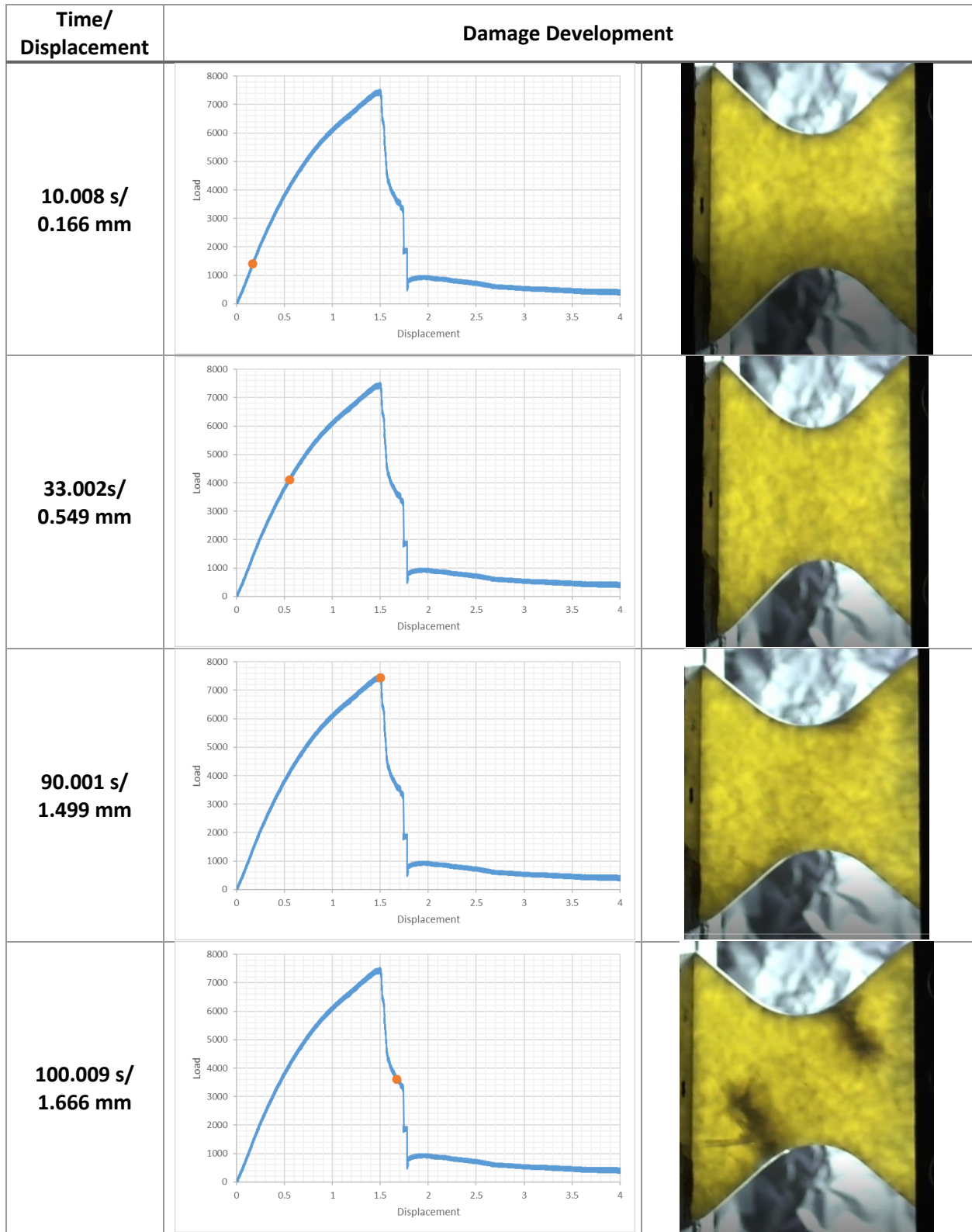
Figure 2.14: Damage development in Arcan specimen at 90º
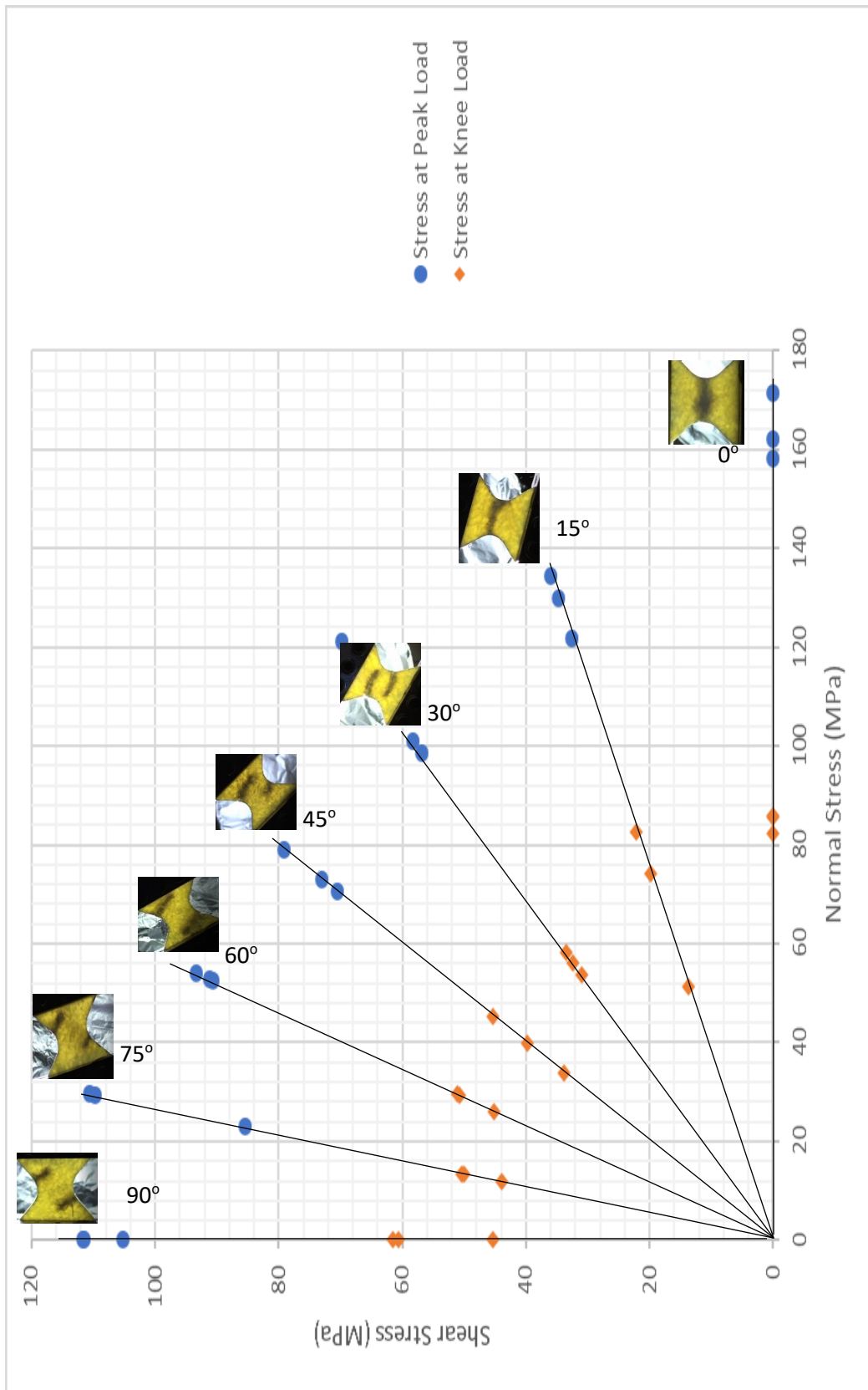
stress plots corresponding t
arious loading angles.

Figure 3.10 plots the normal stress vs. shear stress components for each specimen corresponding to the peak load as well as the knee load. The figure also shows the specimen with crack at each loading angle. The normal and shear stresses are obtained by resolving the loads with respect to the specimen orientation and loading axis at peak load as shown in Equations 2.1 and 2.2. The knee load is, approximately, the transition load from linear to non-linear segments. It was obtained by drawing tangents to the two segments of the load-displacement curves using a MATLAB program. It can be observed in Figure 6 that as the loading angle is increased, the shear stress component increased and the tensile stress component at both peak and knee loads decreased. Thus, both tensile strength and knee strength are reduced as shear stress is increased.

2.6 Failure Prediction Model

There are several different failure prediction models for fiber reinforced composite materials. One common failure prediction model is called the Azzi-Tsai-Hill theory [11] which uses a quadratic equation to predict failure in an orthotropic lamina containing unidirectional fibers. According to this theory, occurs in the lamina when

$$\frac{\sigma_{11}^2}{S_{Lt}^2} - \frac{\sigma_{11}\sigma_{22}}{S_{Lt}^2} + \frac{\sigma_{22}^2}{S_{Tt}^2} + \frac{\tau_{12}^2}{S_{LTs}^2} = 1 \qquad (2.3)$$

where, σ_{11} and σ_{22} are the tensile normal stresses and τ_{12} is the shear stress in the 1-2 directions of the lamina. S_{Lt} and S_{Tt} are the longitudinal and transverse tensile strengths and S_{Lts} is the shear strengths of the lamina. Equation (2.3) is applied if both σ_{11} and σ_{22} are tensile stresses. If σ_{11} is tensile and σ_{22} is compressive, S_{Tt} in Equation (2.3) is replaced with S_{Tc} which represents the transverse compressive strength of the lamina.

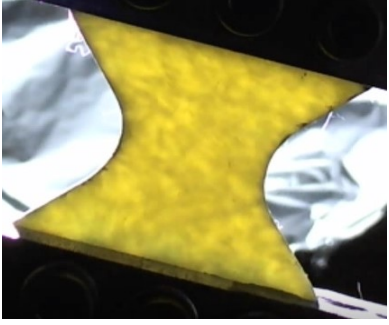Since the SMC-R composite contains randomly oriented short fibers and the fiber length is much greater than its thickness, it, in general, behaves as a planar isotropic material. For such a material, S_{Tt} is equal to S_{Lt}, and the Azzi-Tsai-Hill failure criterion given by Equation (2.3) then transforms into the classical von-Mises failure criterion given by Equation (2.4).

$$\left[\sigma_1^2 - \sigma_1\sigma_2 + \sigma_2^2\right]^{1/2} = S \qquad (2.4)$$

Equation (2.4) is the most commonly used failure model for predicting yielding in an isotropic ductile material. In the case of a planar isotropic material, σ_1 and σ_2 in Equation (2.4) are the principal stresses in the plane of isotropy and S is the failure strength of the material, also in the plane of isotropy.

Due to the nature of the processes involved in making sheet molding compound sheet and resin flow during compression molding of the material into a composite part, it is possible that there are preferred orientations of short fibers in the major flow direction, which, in turn, may cause slight anisotropy in the molded part. In order to predict failure in such a material, a quadratic failure criterion proposed by Hill [9] is applied here. The Hill equation given by Equation (2.5) takes into consideration the anisotropy in the material and introduces two anisotropy ratios R and P in principal stress coordinates.

$$\left[\frac{R}{(1+R)}(\sigma_1 - \sigma_2)^2 + \frac{R}{P(1+R)}\sigma_2^2 + \frac{1}{(1+R)}\sigma_1^2 \right]^{1/2} = S \tag{2.5}$$

Anisotropy ratios R and P are defined as,

$$R = \frac{d\epsilon_2}{d\epsilon_3}$$

$$P = \frac{d\epsilon_1}{d\epsilon_3}$$

where, the strains are obtained by uniaxial testing in directions 1 and 2.

In Equations (2.4) and (2.5), σ_1 and σ_2 are the in-plane principal stresses calculated using σ_{xx} and τ_{xy} corresponding to the failure load, and S is the uniaxial tensile strength of the material. In Equation (2.5), R and P are the anisotropy ratios in three principal stress directions. Note that Equation (2.5) transforms into Equation (2.4) for $R = P = 1$. For a planar isotropic material, $R = P$, and Equation (2.5) transforms into Equation (2.6). Note that Equation (2.6) transforms into Equation (2.4) for $R = P = 1$.

$$\left[(\sigma_1 - \sigma_2)^2 + \sigma_2^2 + \sigma_1^2 \right]^{1/2} = (1+R)^{1/2} S \tag{2.6}$$

The principal stresses corresponding to peak loads and knee loads are plotted in Figures 2.16 and 2.17, respectively. They represent the failure envelopes at these two events. In addition to the test data, Equations (2.4) and (2.6) are also plotted in Figures 2.16 and 2.17. Note that for the tests conducted in this study, σ_1 is a positive principal stress and σ_2 is a negative principal stress. Equation (2.5) is plotted with $P = R = 0.5$ and 2. It is assumed that S is the strength value corresponding to the mean peak load in Figure 2.16 and the mean knee load in Figure 2.17, both at 0° loading angle. It is also assumed that the compressive strength of the material is equal to its tensile strength so that the value of S is the same in both uniaxial tension and compression. It can be observed from Figures 2.16 and 2.17 that there is a large amount of scatter in the experimental data. In Figure 2.16, the predicted stresses at the peak loads are observed to be higher at smaller angles (0 to 45°) and lower at larger angles (60 to 90°). At the knee loads, shown in Figure 2.17, the principal stresses calculated from the test data follow the von Mises failure curve much better than the Hill failure curves with R = 0.5 and R = 2.
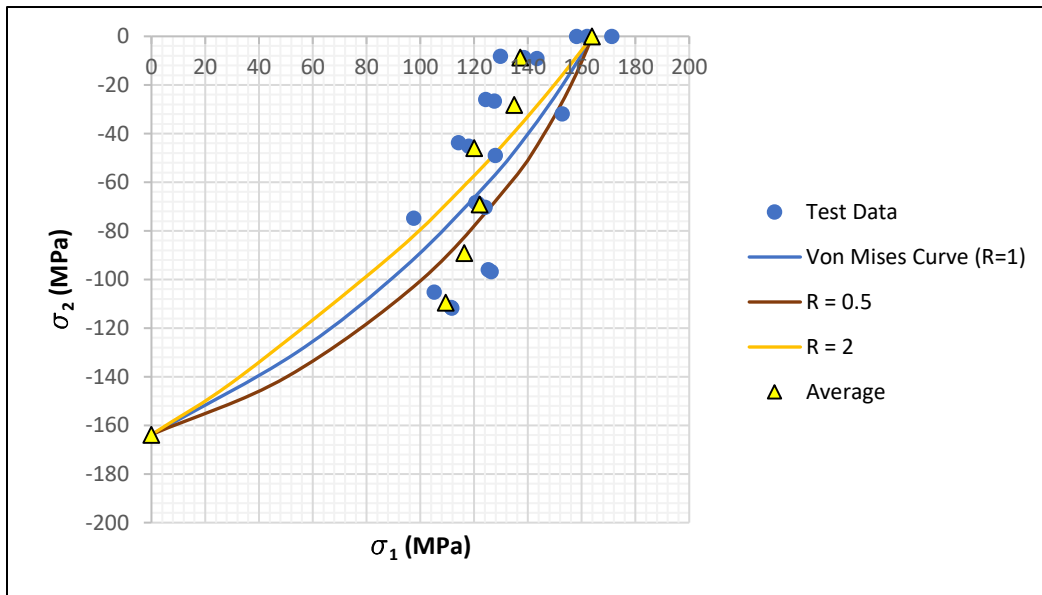
Figure 2.16: Failure envelopes corresponding to the peak load: test data and theoretical prediction using Equations (2.4) and (2.6)
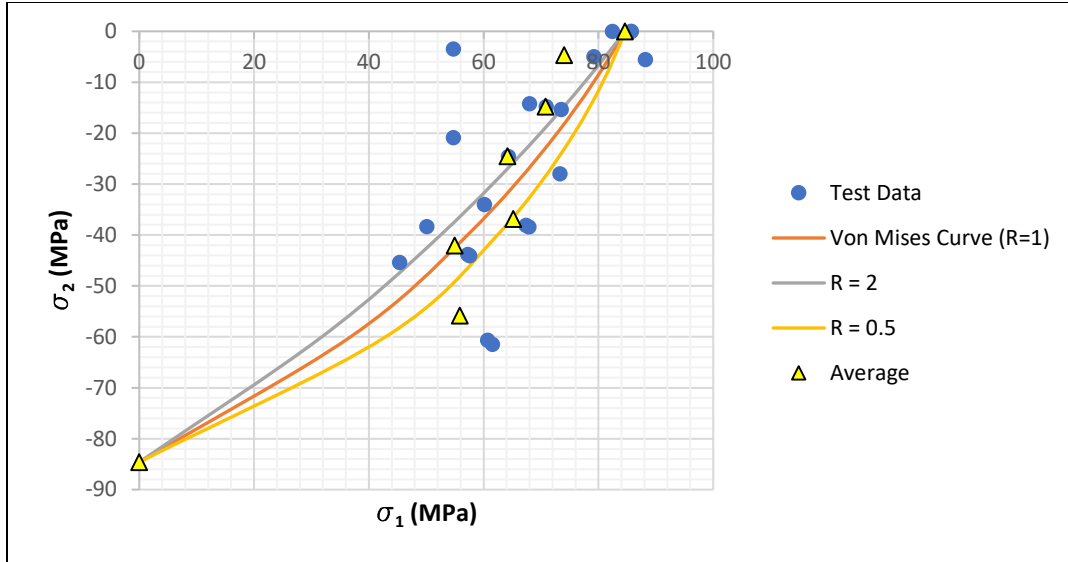
Figure 2.17: Failure envelopes corresponding to the knee load: test data and theoretical prediction using Equations (2.4) and (2.6)

2.7 Microstructure in Failure Region

Analysis of the microstructure is carried out in the failure region to look into the type of damage in the material and the distribution of fiber and matrix. An optical microscope from Leica Microsystems was used for the analysis. The microscope had an objective magnification ranging from 2.5x to 50x and an eyepiece magnification of 10x. A microscope camera was used to capture the images of the microstructure. The camera had a magnification of 2.5x and a pixel density of 2 MP.

Figures 2.18 (a) and 2.18 (b) are images of the microstructure at the failure region. Figure 2.18 (a) shows the crack at the surface and Figure 2.18 (b) shows the crack with the failure in sub surface region. From the two images, it is observed that the crack grows perpendicular to the fiber direction. The damage in the material is a combination of fiber breakage, fiber matrix debonding and matrix failure. The microstructure shows loosely formed fiber bundles instead of individual fibers in the sub surface layers. These bundles are randomly oriented in the matrix.

<div align="center">

(a)   (b)
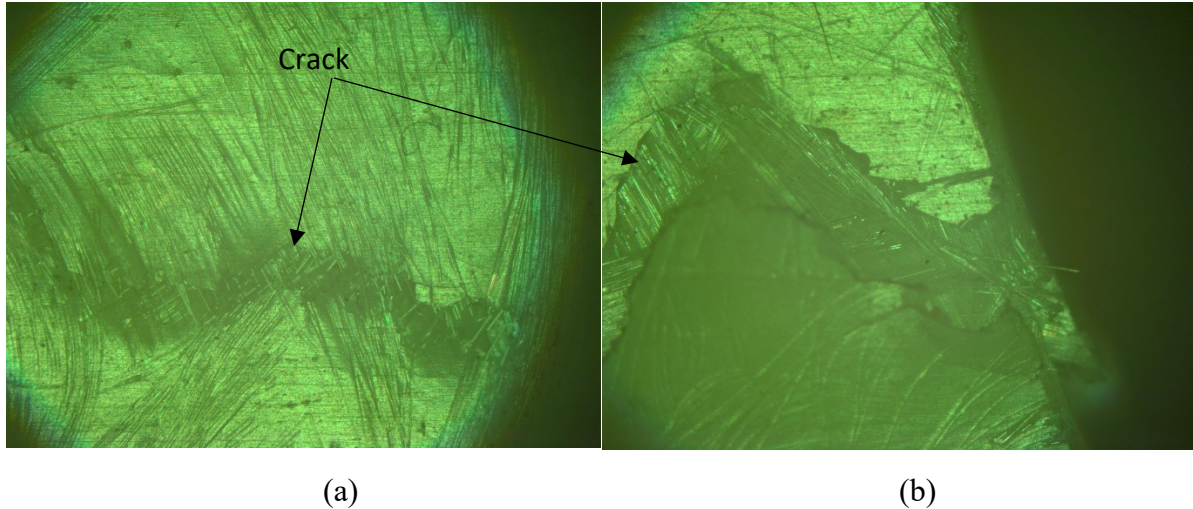
Figure 2.18: Microstructure of glass fiber SMC-R in failure region.

</div>

2.8 Conclusions

1. The load at failure is significantly lower under combined tensile and shear loading conditions compared to uniaxial loading conditions, and is the lowest when tensile and shear loads are equal.

2. Damage development in SMC-R causes the material to change from linear to non-linear behavior as the load is increased and the point of transition is identified as the knee load. The degree of non-linearity increased with increase in shear stress.

3. Tensile and knee strength of the SMC-R composite decrease with increasing shear stress.

4. The von Mises and Hill failure prediction models have not provided a good fit to the biaxial principal stress data at peak loads. However, von Mises failure criterion seems to work reasonably well for the prediction of knee loads where the damage initiation occurs.

CHAPTER 3

STATIC BEHAVIOR OF CARBON FIBER SMC-R IN BIAXIAL LOADING

This chapter considers the behavior of carbon fiber SMC-R under static biaxial loading conditions. The results of the quasi-static biaxial tests are presented and conclusions are drawn.

3.1 Introduction

Carbon fiber composites have lower density, higher strength and higher modulus compared to glass fiber composites. A lot of research has been done on the development of carbon fiber composites due to their immense weight saving potential. Continuous carbon fiber composites are already in use in many aerospace applications and is being developed as an alternative for steels in structural automotive applications. Discontinuous carbon fiber composites, such as carbon fiber SMC, are also being considered in many aerospace and automotive applications, since they not only provide weight saving, but also manufacturing cost reduction due to relatively rapid manufacturing processes that can be used for making them. Discontinuous carbon fiber SMC is currently used in the window frames of ~~the~~ Boeing 787. In the automotive industry, Daimler Chrysler, used 8 kilograms of carbon fiber SMC in its performance vehicle, Dodge Viper. The components included door panels, fender supports, wind shield inner and outer support panel and headlamp supports [26]. It was also used on a trial basis in the Lincoln MKS hood, and an additional weight saving of 42% was observed compared to conventional glass fiber SMC.

Because of increasing interest in carbon fiber SMC for future applications in both aerospace and automotive industries, it is important that its mechanical characteristics are understood and taken into consideration in their design. In recent years, several studies were conducted on the influence of defects on crack initiation [27, 28]. The study reported by Feraboli et al. on the influence of defects in carbon fiber SMC observes that crack initiation in carbon fiber

SMC cannot be directly related to defect locations. However, these defects do influence crack initiation due to differential strains in the region. In general, failure in Carbon fiber SMC is observed to be caused due to fiber breakage, inter- laminar failure or fiber matrix debonding. Most of these studies are concentrated on uniaxial tensile or flexural behavior of the material.

This chapter focuses on the strength and failure characteristics of Carbon fiber SMC-R under different biaxial loading conditions. A series of quasi-static and fatigue tests were conducted using butterfly shaped Arcan specimens. The results of the quasi-static tests are reported in this chapter. The results of the fatigue tests are reported in Chapter 4.

3.2 Material

The material used in this study is a Carbon fiber reinforced epoxy molding compound supplied by Quantum Composites, an A. Schulman Company. The fiber type in the material is 3K PAN carbon and the nominal fiber content is 52% by weight. A mix of 25 and 50 mm long carbon fibers is used. This material is under development for commercial use in North America, Asia, and Europe. The properties of the material as mentioned in its product literature are listed in Table 3.1.

3.2.1 Processing of Composite

Ten carbon fiber SMC-R plates, each 30 cm by 30 cm with a nominal thickness of 3.18 mm, were obtained from Quantum Composites. Such plates are manufactured in a two-step process. In the first step, a mixture of 25 and 50 mm chopped carbon fibers are impregnated by the epoxy resin and stored as rolls. These rolls are cut into the desired shape and placed in a compression molding machine. The SMC-R composite is molded at temperatures in the range of 127-163 °C, with 149 °C suggested as a starting point. Cure time is typically 6-10 minutes; it depends on mold temperature and part thickness. The part is then cooled at room temperature.

Table 3.1: Properties of carbon fiber SMC-R.

Physical	Value	Unit
Density	1.45	g/cm^3
Shrinkage	-0.001	in/in
Poisson's Ratio	0.33	-
Mechanical	**Value**	**Unit**
Tensile Modulus	37,921	MPa
Tensile Stress (at Break)	290	MPa
Flexural Modulus	34,473	MPa
Flexural Stress (at Break)	538	MPa
Compressive Stress (at Break)	276	MPa

3.3 Test Procedure

3.3.1 Specimen

The quasi-static and fatigue tests of Carbon fiber SMC-R were conducted using butterfly shaped Arcan specimens shown in Figure 3.1. Its dimensions are given in Chapter 2. The specimen has a nominal cross-sectional area of 74.0304 mm^2 at the significant section.

3.3.2 Test Procedure

The quasi-static test procedure is the same as the procedure followed for glass fiber SMC-R. For Carbon Fiber SMC-R, additional tests are conducted at each loading angle, especially at 0° to document the variations in properties. Due to the opacity and surface reflectivity of the specimen, video was not taken during the course of the test. The machined edges of the specimen are smoothened with coarse and fine sand papers to remove any imperfections from machining. The bolts holding the specimen in the fixture are tightened to a torque value of 15 N.m.

Figure 3.1: Carbon fiber SMC-R specimen

3.4 Results

3.4.1 Quasi-Static Biaxial Test Results

To understand the behavior of Carbon Fiber SMC-R under biaxial load, the butterfly shaped Arcan specimen were tested at 0°, 30°, 45°, 60° and 90°. The tests at 0° and 90⁰ represent uniaxial tensile and pure shear test conditions, respectively. The peak load recorded for each specimen is shown in Table 3.2. Decrease in peak load with increase in loading angle is similar to the behavior, seen for glass fiber composite in Chapter 2. The decrease is sharp with the introduction of shear stress to the specimen as seen for 30° specimens versus the 0° specimen; but, above 45°, the peak load becomes stable. The knee load has also decreased with increasing loading angle, though perhaps not as significantly as the peak load.

The crack development in the carbon fiber specimens varied depending on the loading angle. Figure 3.2 shows the damage in specimen at different loading angles. A single crack is seen to develop at the critical section or close to it and propagates across the width with an increase in load. The crack propagates at an angle to the width under biaxial and shear stress, as seen in Figure 3.2. Under pure shear, two cracks are observed similar to the glass fiber specimens.

The failure in material is observed to occur due to fiber pull-out resulting from a tensile stress. Under biaxial load, the tensile stress is local to the crack initiation location and creates a corresponding compressive stress at the opposite side. Under pure shear, the failure mode is

observed to differ due to the higher compressive load resulting in interlaminar debonding along with fiber pull-out and fiber matrix debonding, as shown in Figures 3.2 (c) and (d). As the crack propagates, it takes the path of least resistance. And, due to various factors such as fiber distribution, fiber-matrix bonding and inter laminar strength, crack propagation is not identical at each loading angle and in some cases crack was observed at bolt holes too.

Table 3.2: Peak and Knee loads at each test condition.

Specimen No.	Loading Angle (deg)	Peak Load (kN)	Average Peak Load (kN)	Knee Load (kN)	Average Knee Load (kN)
SMCR-CF-011-ST	0	23.32	21.87	5.5	5.33
SMCR-CF-012-ST	0	21.18		5.6	
SMCR-CF-013-ST	0	23.95		5.4	
SMCR-CF-014-ST	0	18.39		4.8	
SMCR-CF-301-ST	30	13.92	14.27	4.2	4.20
SMCR-CF-302-ST	30	15.12		4.3	
SMCR-CF-303-ST	30	16.78		4.3	
SMCR-CF-304-ST	30	11.24		4	
SMCR-CF-451-ST	45	15.66	13.14	4.8	4.14
SMCR-CF-452-ST	45	10.52		4.7	
SMCR-CF-453-ST	45	12.03		4	
SMCR-CF-454-ST	45	13.86		3.5	
SMCR-CF-455-ST	45	13.60		3.7	
SMCR-CF-601-ST	60	9.98	10.64	2.9	3.47
SMCR-CF-602-ST	60	10.79		4	
SMCR-CF-603-ST	60	11.14		3.5	
SMCR-CF-901-ST	90	11.198	10.68	3.5	3.10
SMCR-CF-902-ST	90	10.16		2.7	
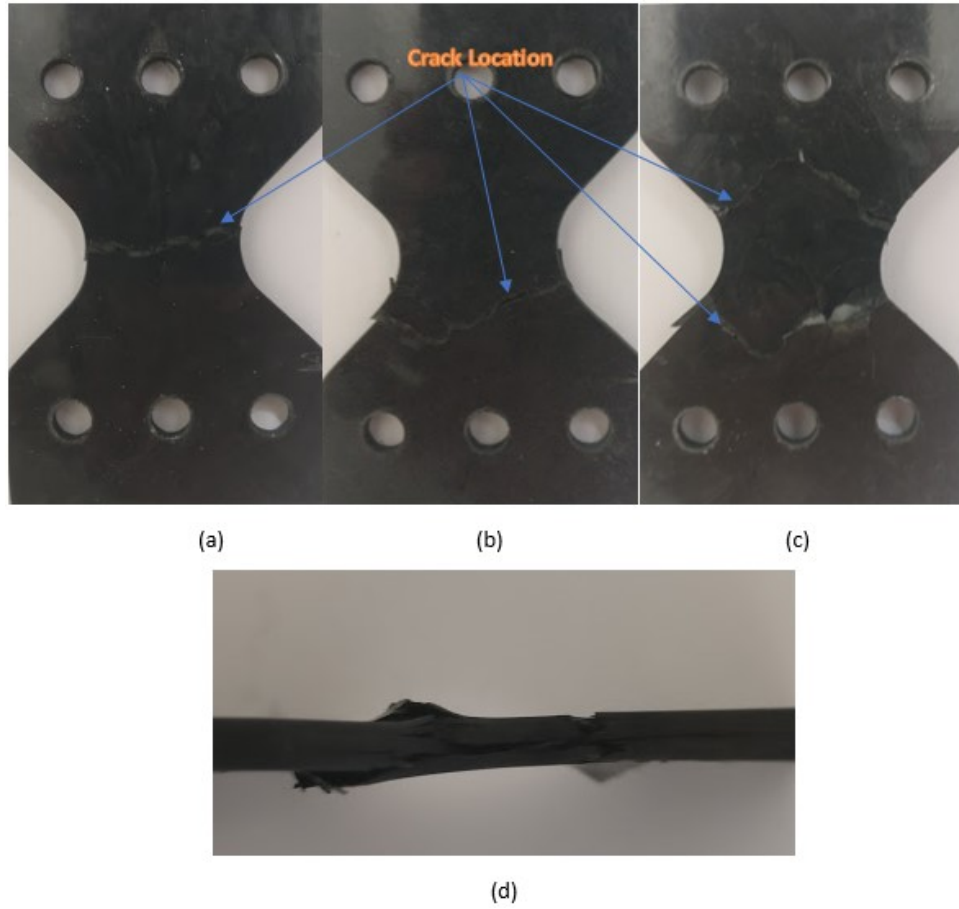
Figure 3.2: Crack location at (a) 0º, (b) 30º to 60º, (c) and (d) 90º
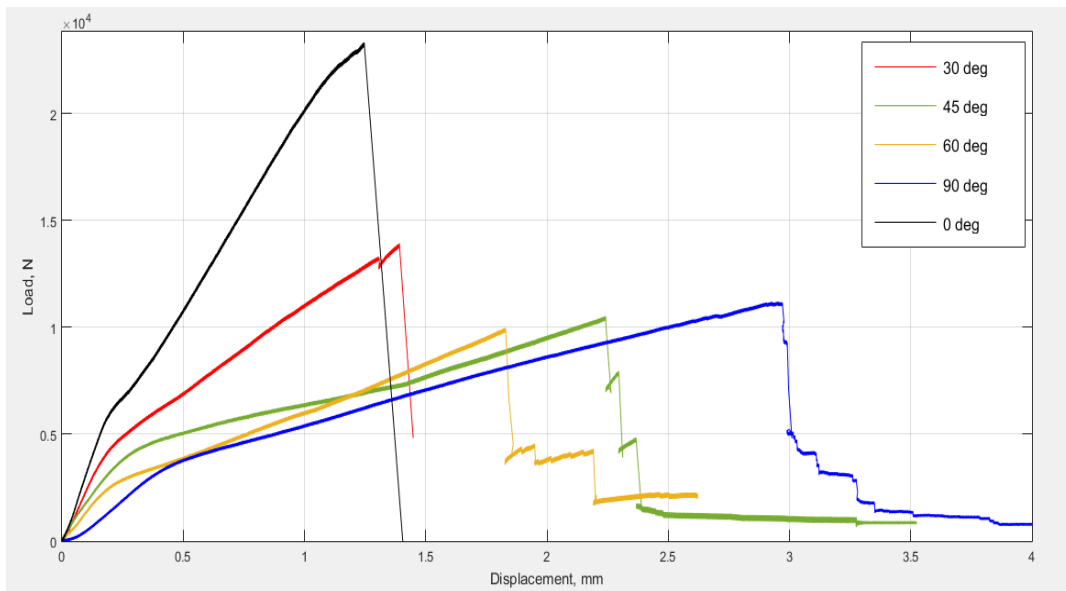
Figure 3.3: Load – displacement curves for carbon fiber SMC-R

Figure 3.3 illustrates a comparison of load displacement curves at different loading angles. The curve for the carbon fiber composites shows two linear segments with different slopes; however, with less non-linearity compared to glass fiber SMC in Chapter 2. The change in slope is more pronounced compared to glass fiber composites. The slope of the curve decreases with an increase in the loading angle.

Figure 3.4 plots the normal stress vs. shear stress values corresponding to peak and knee loads at different loading angles. The normal stress and shear stresses were calculated using Equations (2.2) given in Chapter 2. This plot clearly shows the quadratic nature of the effect of biaxiality on the strength of carbon fiber SMC. The peak stress at 0° loading angle represents the tensile strength of the material, while the peak stress at 90° loading angle represents its shear strength. From Figure 3.4, it can be observed that the tensile strength of the material decreases with increasing shear stress and the shear strength of the material decreases with increasing tensile stress in a biaxial stress field

Figure 3.4: Shear stress vs. normal stress plots corresponding to peak

loads at various loading angles for Carbon Fiber SMC
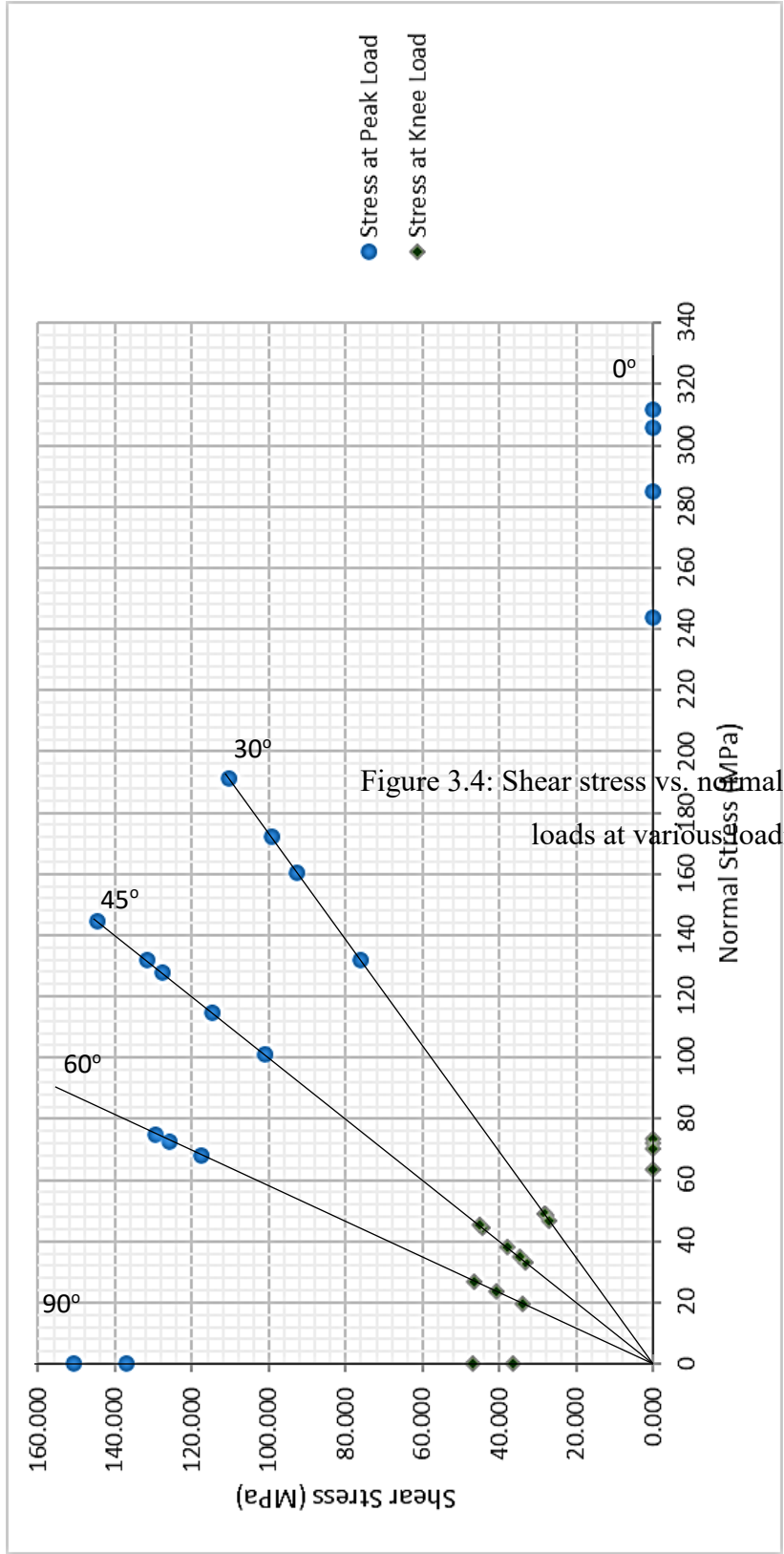
3.4.2 Statistical Analysis for Quasi-Static Results

3.4.2.1 Tensile Tests

Previous studies as explained in Chapters 1 and 2 have shown that SMC-R composites have tendency to show variations in properties. These findings are reinforced by the results seen in the previous section. Therefore, it is important to study the failure stresses of the material using statistics. The variation in failure stresses were largely observed in the tensile and 45° cases. Hence, the results from these two cases have been analyzed using probability distributions.

The specimens for the tensile tests were taken from multiple SMC-R sheets and they were cut at different angles from the sheet. A majority of the specimen were cut at 0°, if one side was assumed to be the x-axis. The results of the tests are shown in Table 3.3. From the data obtained in the 0° Arcan tests for Carbon fiber SMC-R, a wide range of failure loads have been observed. To predict the failure load of composites, it is important to use a parameterized distribution for the data set. Weibull distribution provides a more accurate picture of the strength variation in composites. For the test data obtained a two parameter Weibull statistic was used. The mean strength of the laminate is defined as;

$$\bar{\sigma} = \sigma_0 \Gamma \left(\frac{1 + \alpha}{\alpha} \right)$$

$$\dots (3.1)$$

where, σ is the mean strength, σ_O is the location parameter (MPa), and α is the dimensionless shape parameter. The probability of failure P given by Equation (3.2) and Y_p given by Equation (3.3) are used to calculate the location parameter and shape parameter. The expressions for the probability functions are,

$$P = \frac{i}{(1+n)}$$

$$\dots (3.2)$$

$$Y_p = \ln\{\ln\left[\frac{1}{(1-P)}\right]\}$$

$$\dots (3.3)$$

Table 3.4 shows the maximum stress data with values of the probability functions. This data is plotted in Figures 3.5 and 3.6. Figure 3.5 plots the probability of failure against the strength of each specimen obtained from test results. Figure 3.6 is plotted to obtain the shape parameter

and location parameter for the Weibull distribution. From Figure 3.6 using Weibull distribution technique, we get the mean tensile strength as follows,

Slope, $\alpha = 8.7434$ and $\sigma_o = e^{5.60194} = 270.9515$

And, Mean tensile strength, $\sigma = \sigma_o\ \Gamma(9.7434/8.7434) = \underline{256.24\ \text{MPa}}$

The crack development for the tensile test specimens is the same macroscopically when comparing specimens which failed at different peak loads. There is no variation observed apart from minor variation in path of crack propagation, which is expected due to fiber orientation and distribution in matrix. In general, the crack initiates at one end of the critical section and grows along the width if the specimen. A failed tensile test specimen is shown in Figure 3.7.

Table 3.3: Failure loads obtained for uniaxial tensile testing.

Specimen no.	Area of Significant Section (mm^2)	Angle at which specimen is cut (º)	Failure Stress (MPa)
Plate 1			
SMCR-CF-001-ST	75.8602	0	237.28
SMCR-CF-002-ST	75.8276	90	217.59
SMCR-CF-003-ST	75.8602	30	246.51
SMCR-CF-004-ST	75.6275	0	224.78
SMCR-CF-005-ST	75.14	90	259.52
SMCR-CF-006-ST	74.5362	0	221.37
SMCR-CF-007-ST	74.9037	90	225.62
SMCR-CF-008-ST	74.9012	45	269.69
SMCR-CF-009-ST	74.7684	45	284.88
SMCR-CF-010-ST	74.6396	0	198.29
Plate 2			
SMCR-CF-011-ST	76.2188	0	305.69
SMCR-CF-012-ST	76.4853	0	285.02
SMCR-CF-013-ST	76.9202	0	310.71
SMCR-CF-014-ST	75.5244	0	244.95
Plate 3			
ST021	72.6596	0	276.5
ST024	71.764	0	287
ST042	73.4806	0	250.9
ST051	73.162	0	259.2
Plate 4			
ST032	74.1146	0	270

Table 3.4: Strength Data with their Probability

i	σ	P	Y_p	ln σ
1	198.286	0.048	-3.020	5.290
2	217.599	0.095	-2.302	5.383
3	221.369	0.143	-1.870	5.400
4	224.786	0.190	-1.554	5.415
5	225.623	0.238	-1.302	5.419
6	231.451	0.286	-1.089	5.444
7	237.279	0.333	-0.903	5.469
8	246.506	0.381	-0.735	5.507
9	250.900	0.429	-0.581	5.525
10	259.200	0.476	-0.436	5.558
11	259.516	0.524	-0.298	5.559
12	269.689	0.571	-0.166	5.597
13	270.000	0.619	-0.036	5.598
14	276.500	0.667	0.094	5.622
15	278.500	0.714	0.225	5.629
16	284.880	0.762	0.361	5.652
17	287.000	0.810	0.506	5.659
18	285.022	0.857	0.666	5.653
19	305.699	0.905	0.855	5.723
20	310.712	0.952	1.113	5.739
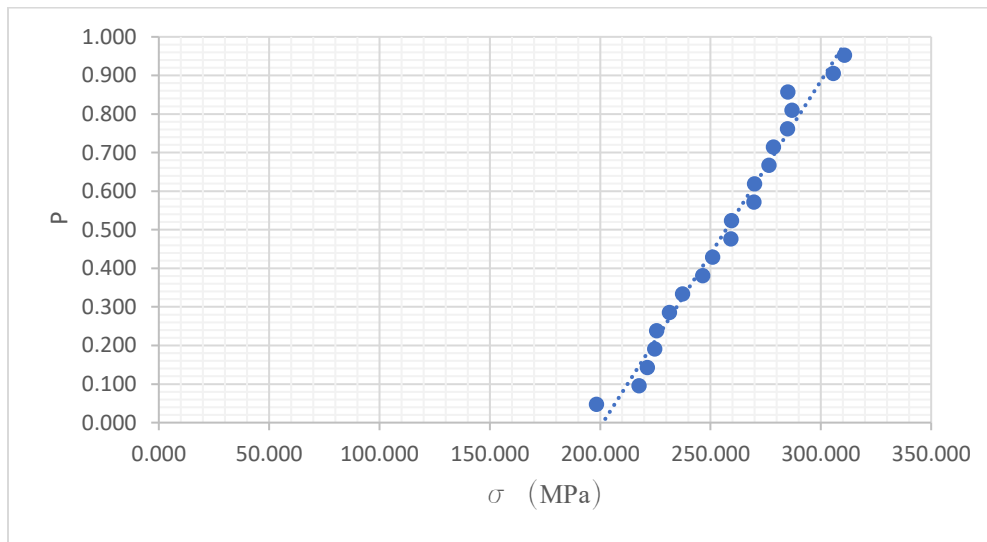
Figure 3.5: Probability of failure vs strength of composite for tensile tests.

46
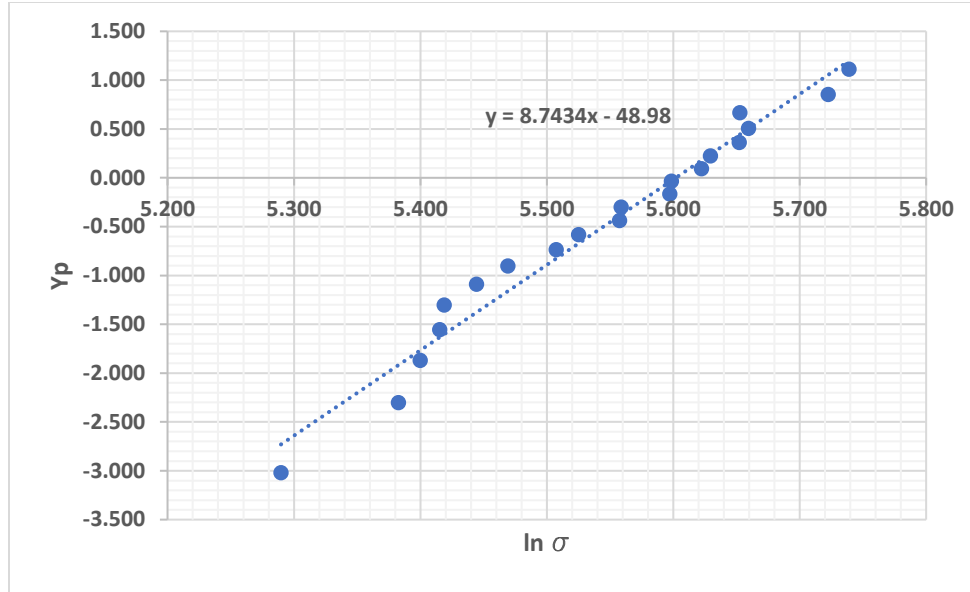
Figure 3.6: Y_p vs ln σ for tensile tests.

3.4.2.2 Biaxial Tests at 45°

The specimens tested at 45° showed a similar variation in the failure stress. The two parameter Weibull distribution is used to determine the failure stress in this case too. Since, this is a biaxial load case, with equal normal and shear stresses, the normal stress is considered to obtain mean stress. Table 3.5 shows the failure stress data with their probabilities. This data is plotted in Figures 3.8 and 3.9. Figure 3.8 plots the strength of the specimen versus probability of failure and Figure 3.9 plots the probability distribution parameters. From the distribution plots using Weibull distribution formulae, we get the mean strength to be

Slope, $\sigma_o = e^{4.884} = 132.1$

And, Mean Normal/Shear strength, $\sigma = \sigma_o \Gamma(5.884/4.884) = \underline{121.19 \text{ MPa}}$

Figure 3.7: Damage in Carbon Fiber SMC-R under tensile load.

Table 3.5: Strength Data with their Probability

i	σ	P	Y_p	ln s
1.000	101.198	0.167	-1.702	4.617
2.000	114.749	0.333	-0.903	4.743
3.000	127.535	0.500	-0.367	4.848
4.000	131.712	0.667	0.094	4.881
5.000	144.663	0.833	0.583	4.974
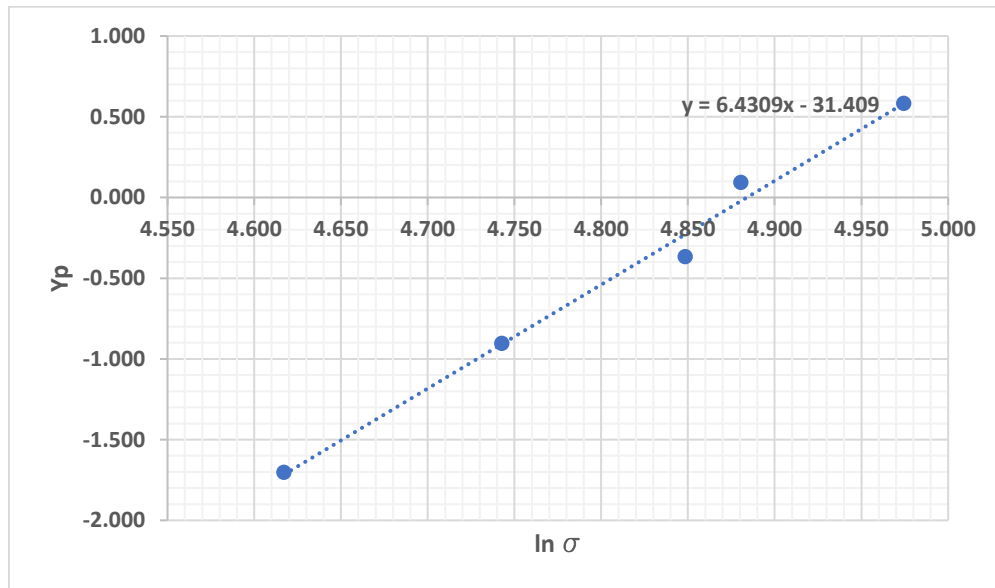
Figure 3.8: Probability of failure vs strength of composite for 45° Tests
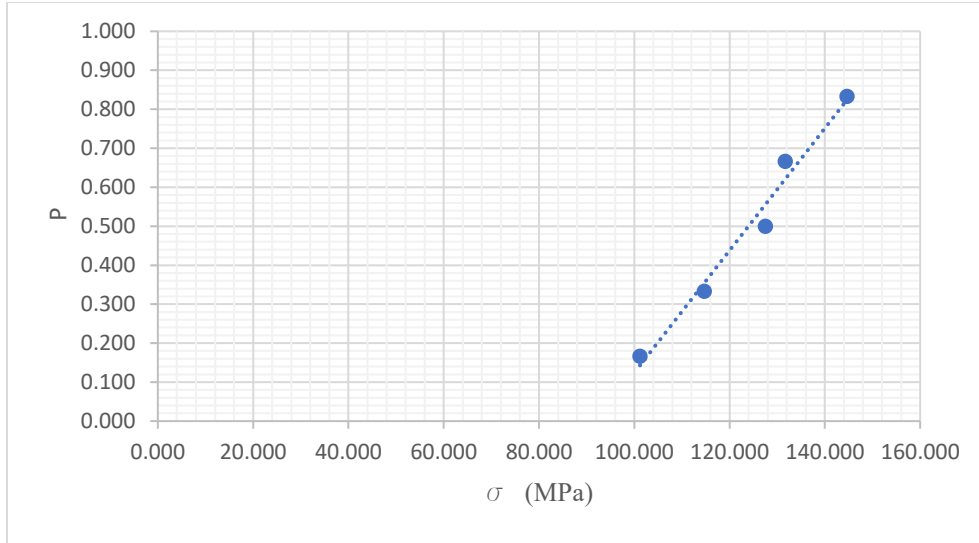
Figure 3.9: Y_p vs ln σ for 45º tests.

3.5 Failure Prediction

Von Mises and Hill's failure prediction model are applied to the data generated for the Carbon fiber SMC-R. The failure prediction model for the peak load principle stresses are plotted in Figure 3.10. And, the failure prediction model at knee load stresses is shown in Figure 3.11. For the peak load failure prediction model design stress is taken to be the stress calculated from the Weibull distribution and at the knee load, the design stress is assumed to be the average value.

Despite scatter in the data, the data points are observed to follow the failure prediction models in Figure 3.8. Hill's failure criterion with an anisotropy ratio of 2 is seen to represent the average of the test data more closely. However, neither can accurately stand for the lower bound of the test data. The lower limit of the strength data is seen to drop significantly when shear stress is introduced at 15º loading angle.

At the knee load, Hill's failure prediction model with P = R = 2 is seen to predict the lower bound of the test data quite closely. While, Hill's equation with an anisotropy ratio of P = R=0.5 is seen to closely follow the average test values. There is no one prediction method which can accurately represent peak load as well as knee load.
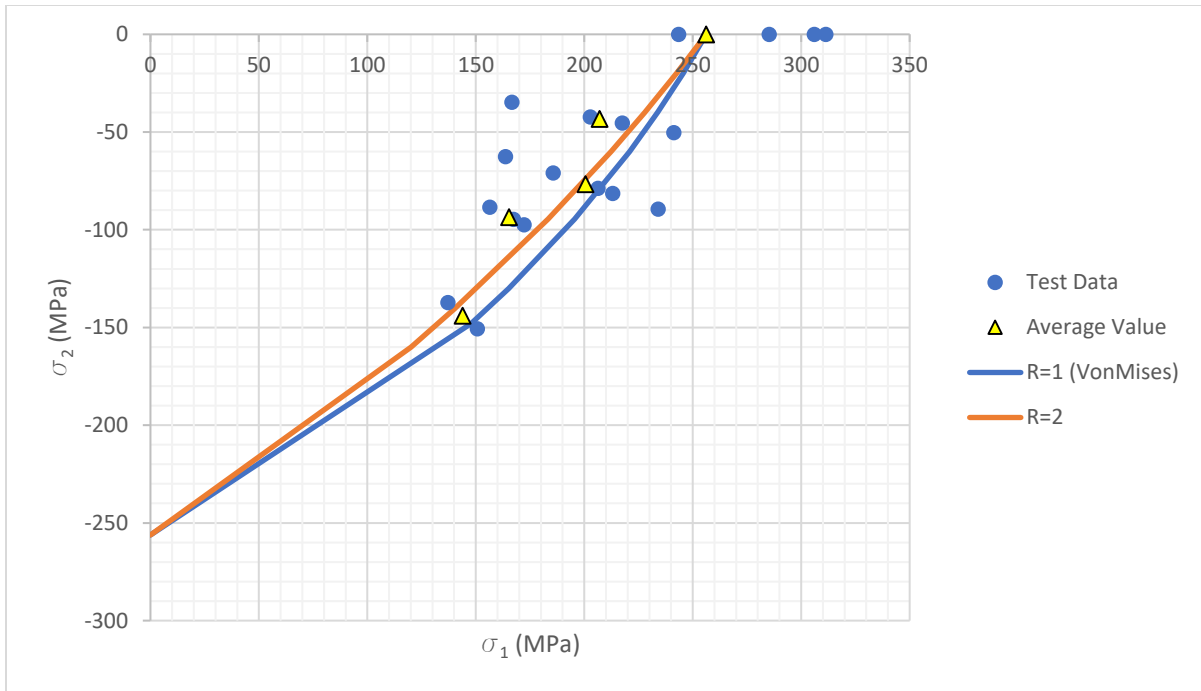
Figure 3.10: Failure prediction envelope at peak load.
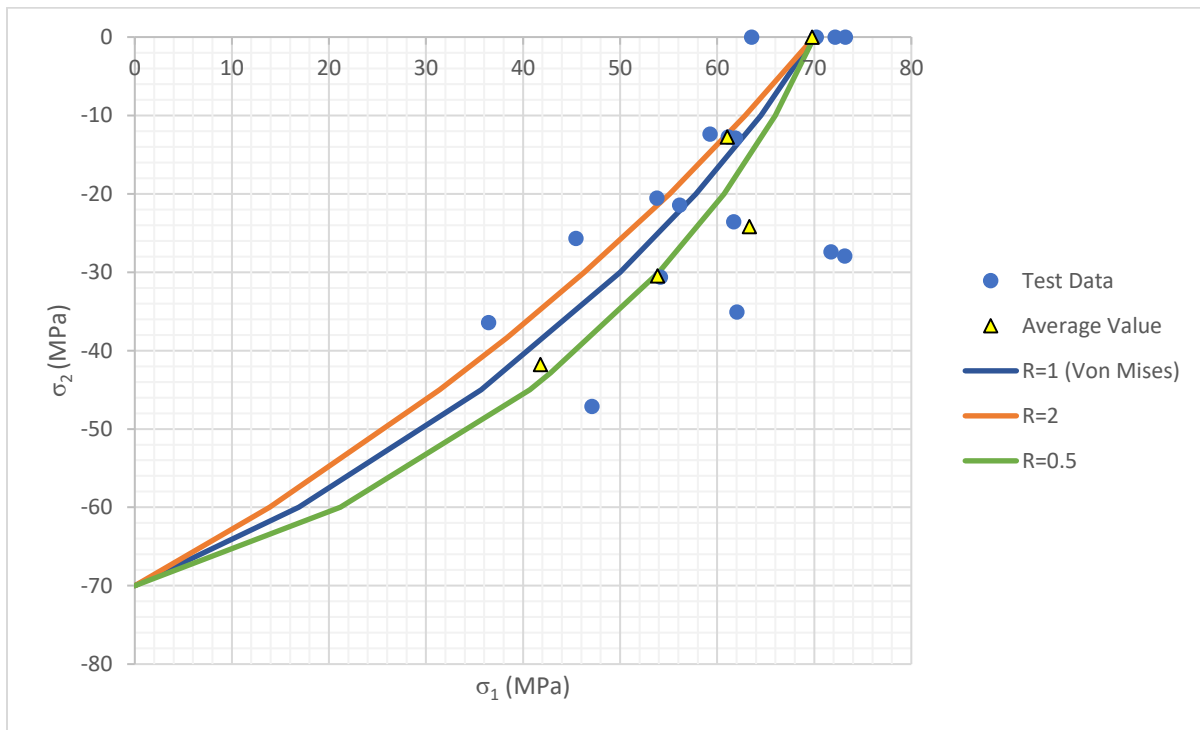
Figure 3.11: Failure prediction envelope at knee load.

3.6 Microstructure in Failure Region

The microstructure of the material in the failure region is analyzed to understand the types of failure, direction of crack growth and fiber-matrix distribution in the material. Figures 3.12 (a) and 3.12 (b) show the thickness-direction view of a shear specimen in its failure region. It can be observed that that the failure in this case was due to multiple short-range delamination which took place in a zig-zag fashion. Even though there were only three layers in the charge, non-uniform movement of fibers and matrix in the thickness direction during compression molding has created multiple layers of interlaminar weakness which is possibly the reason for such failure.

The fiber orientation and distribution in the failure region is shown in Figures 3.13 (a) and 3.13 (b). The crack growth is seen to occur transverse to the fiber orientation as observed in Figure 3.13 (b). The fibers are observed to be in the form of bundles, and these bundles are oriented randomly in the matrix as seen in Figure 3.13 (a). Failure is observed to occur due to fiber matrix debonding, fiber failure and matrix failure.

(a)

(b)
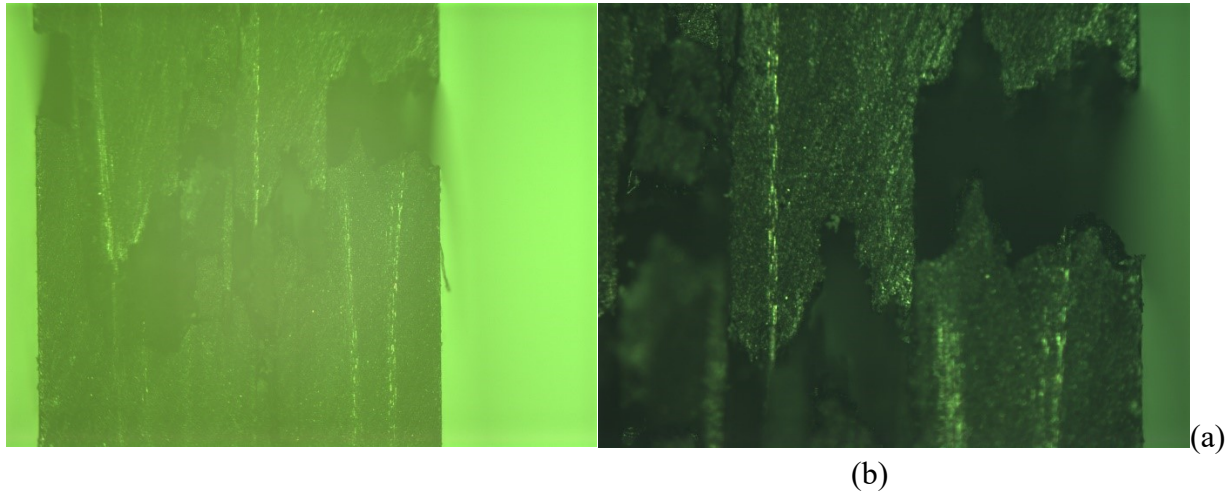
Figures 3.12: Thickness-direction view of carbon fiber SMC-R in the failure region.
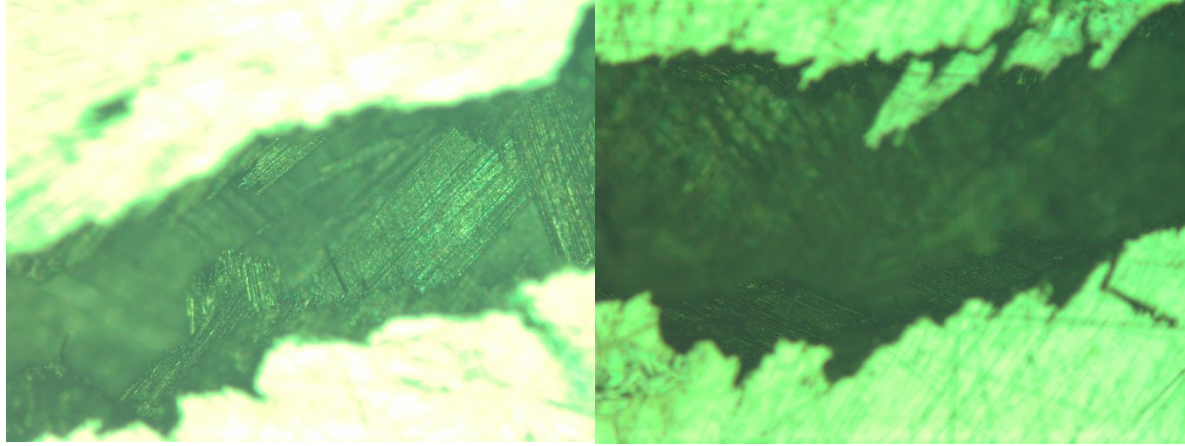
<div align="center">(a) Sub surface view   (b) Surface view</div>

Figure 3.13: Fiber orientation and distribution of carbon fiber SMC-R in the failure region.

3.7 Finite Element Analysis

Finite element analysis is used to study the stress distribution in the specimen under different load cases. The test results have shown that a change in loading angle results in a change in the location of crack initiation. Also, the location of crack initiation in biaxial and shear cases is offset from the critical section. Therefore, to understand the reason behind this, FEA is used.

3.7.1 Finite Element Model

Figure 3.14 illustrates the finite element model of the test setup including the test fixture and specimen. The fixture and the specimen are modelled using tria or quad shell elements. The material for both specimen and loading fixture is defined as linear isotropic. In the case of the specimen, it is defined as linear isotropic, since the simulation is carried out only in the linear region of the material, i.e. load applied is below the knee load of the material and the material is assumed to be isotropic. The fixture elements had a thickness of 9 mm with three through thickness integration points. Since, analysis is mainly concentrated on the stress distribution under uniaxial and biaxial loads, the properties of the specimen elements were taken to be the same as the Carbon fiber SMC-R properties for all the simulations. The thickness of the specimen elements is 3.18 mm with three through thickness integration points. The specimen is fixed to the loading fixture using fully constrained rigid body elements. The upper fixture is fully constrained and load is

applied to the lower fixture. The lower fixture has a degree of freedom only in the loading direction.

3.7.2 Discussion

Figures 3.15, 3.16 and 3.17 illustrate a comparison between the FEA results and the test results. The figures with FEA results plots the Von Mises stress contour and the corresponding failed specimen at 0°, 45° and 90° shown. From the three figures we can observe that, the development of crack is closely associated with the region of stress concentration. The crack is seen to originate at the region of stress concentration when we compare it with the damage development illustrations shown in Chapter 2.
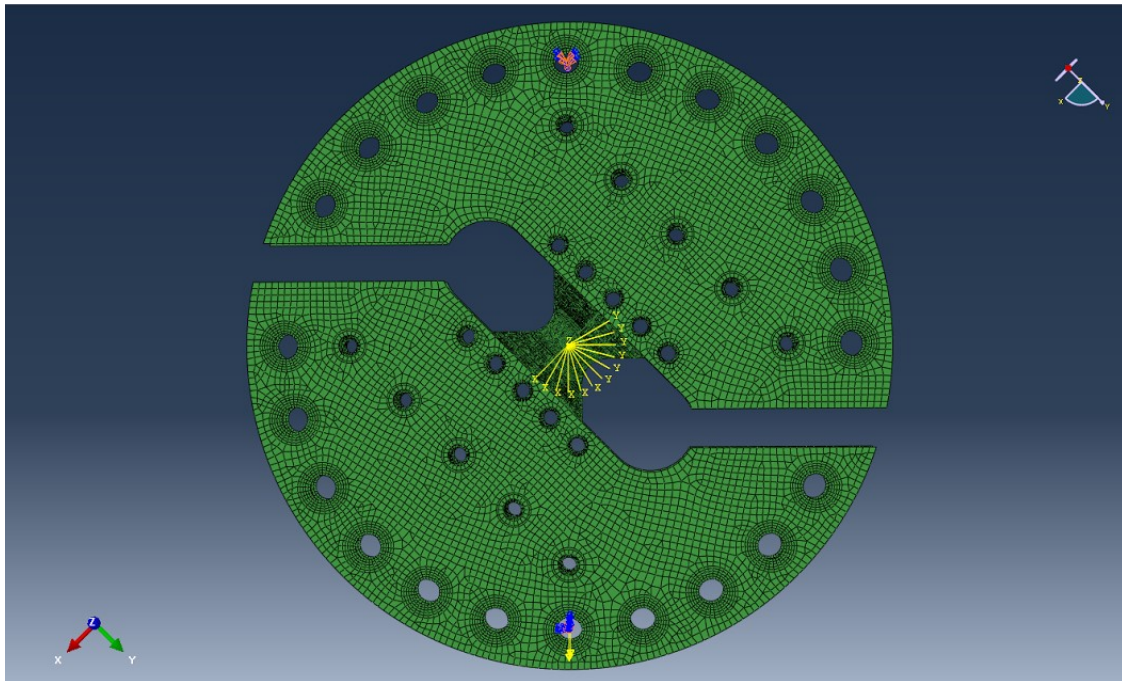
Figure 3.14: Finite Element Model
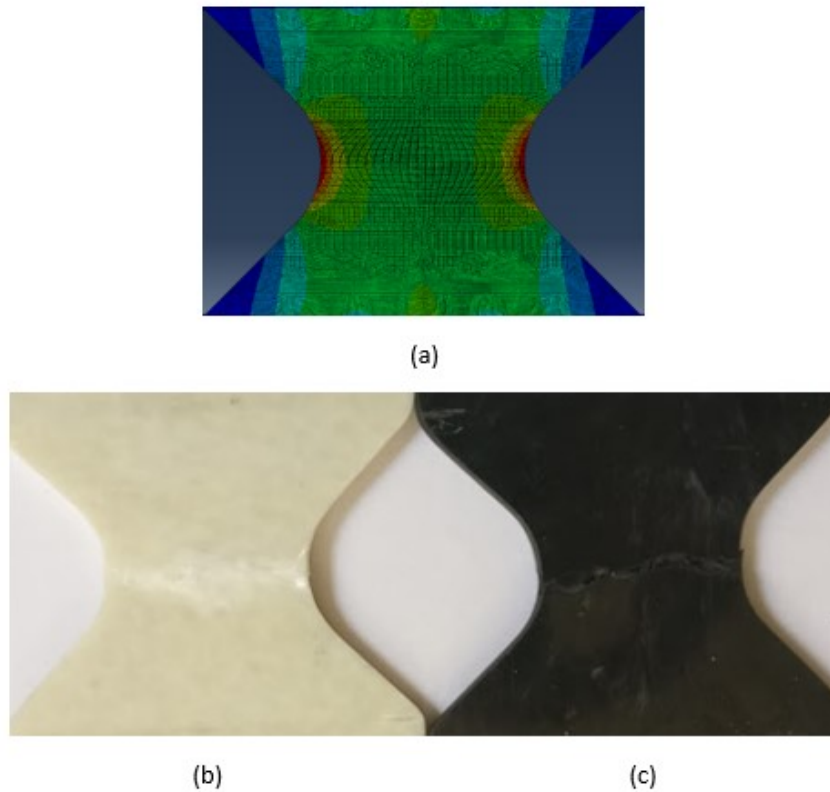
Figure 3.15: Results at 0° Loading Angle.

Similar to observations in test results, the region of stress concentration is seen to move away from the critical section. This data has been recorded and the comparison with test data, shown in Table 3.6. From the table, we can see that the distance shown in FEA, in general, is similar to those observed in physical tests. These regions of stress concentrations are observed to develop due to localized tensile, shear and compressive stresses. These stresses are a result of the test setup. In a biaxial case, when the load is applied, due to the specimen orientation and movement of the loading fixture, the specimen has a tendency to rotate about its center which is stopped by the bolts holding it in place. This generates tensile and compressive stress concentration regions as seen in Figures 3.16 (a) and 3.17 (a). Figures 3.18 and 3.19 show the tensile and shear plots at 45° and 90°. The region shaded in red indicates a tensile stress concentration while blue indicates a compressive stress in figures 3.18(a) and 3.19(a). Figures 3.18(b) and 3.19(b) show the shear stress plot. Despite the influence of peak stress on the crack initiation, the stress distribution across the critical section is seen to be nearly uniform, validating the use of Arcan test method.
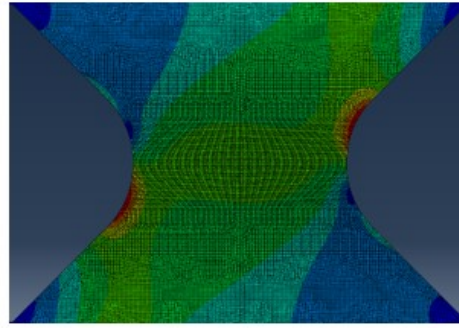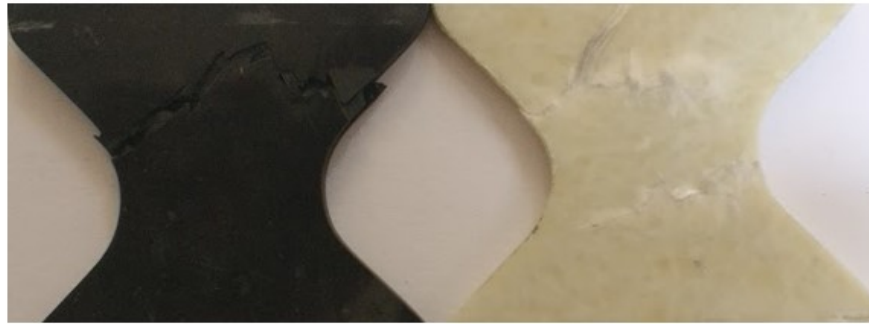
Figure 3.16: Results at 45º Loading Angle.
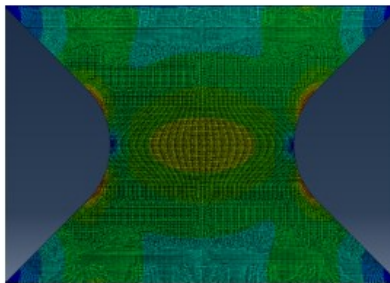
Figure 3.17: Results at 90º Loading Angle.

Table 3.6: Distance of Crack origin from Significant Section in FEA

Specimen No.	Distance from Significant Section	FEA Result
SMCR-001-St	0	0
SMCR-002-St	1.4	
SMCR-003-St	0	
SMCR-151-St	3.2	3.7
SMCR-152-St	4.6	
SMCR-153-St	3.5	
SMCR-301-St	4.7	6.6
SMCR-302-St	4.9	
SMCR-303-St	3.9	
SMCR-451-St	6.2	8.4
SMCR-452-St	7.9	
SMCR-453-St	4.8	
SMCR-601-St	8.4	8.5
SMCR-602-St	7	
SMCR-603-St	6.5	
SMCR-751-St	5.3	8.7
SMCR-752-St	5.1	
SMCR-753-St	4.7	
SMCR-901-St	8.1	8.7
SMCR-902-St	7.6	
SMCR-903-St	8.4	
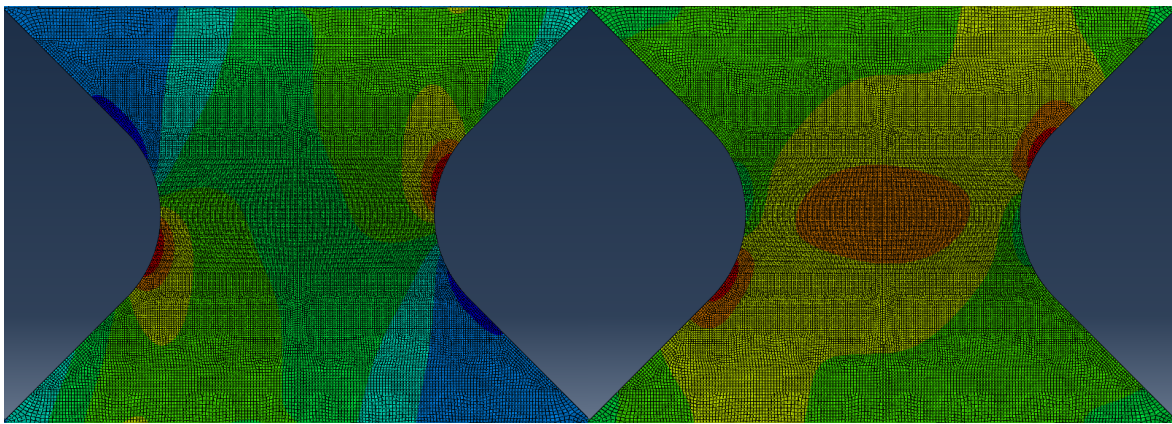
(a)   (b)

Figure 3.18: Contour Plot showing σ_{11} (a) and σ_{12} (b) for 45° case.
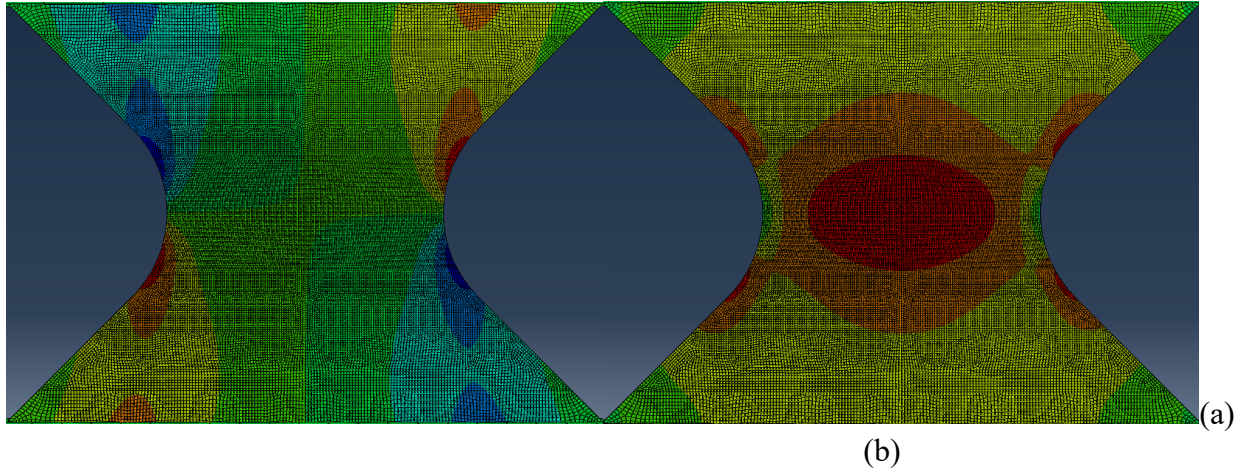
Figure 3.19: Contour Plot showing σ_{11} (a) and σ_{12} (b) for 90º case.

3.8 Conclusions

1. Under Quasi-Static tests, material shows a transition from linear to nonlinear behavior and the point of transition is referred to as knee load. Knee load for carbon fiber SMC-R is seen to be quite low compared to the peak load.

2. Carbon fiber SMC-R shows a similar decrease in the properties under biaxial load. The stiffness if the material in particular, decreases greatly.

3. Two-Parameter Weibull Distribution is used to obtain the strength of material under tensile and Biaxial load due to variation in data.

4. Hill's failure theory is seen to closely follow the test data at the peak loads and knee loads by taking into consideration an anisotropic factor.

CHAPTER 4
FATIGUE BEHAVIOR OF CARBON FIBER SMC-R IN BIAXIAL LOADING

This chapter presents the results of the cyclic fatigue tests conducted on carbon fiber SMC-R under tensile, shear and a combination of tension and shear loading conditions.

4.1 Introduction

Product reliability is important in every industry and hence, most industries invest heavily to investigate it. This is especially so, when new technology or materials are used in a product. The use of composites in a small scale, in niche applications have helped the industry to ensure complete control over the manufacturing process and quality of the material being produced. However, as the material is being introduced to the mass production, it is difficult to maintain process control over the large batches. These variations in tensile fatigue and shear fatigue properties for SMC-R have been documented in previous research [1,4,5]. This makes the study of material reliability very important.

Chapters 2 and 3 have shown that the SMC-R composites do not show uniform properties across the batches. Therefore, the objective of this chapter is to test the material for durability and failure behavior under different loading conditions. The Fatigue tests are conducted using butterfly shaped Arcan specimen using a modified Arcan Test procedure as explained previously. Similar to the quasi static test results, variation is expected in the fatigue test results, hence, different probability distributions are used to obtain the life prediction curves for the material.

4.2 Test Procedure

The second part of the tests conducted on carbon fiber SMC-R is cyclic loading. A few initial fatigue tests conducted at 2 Hz and a maximum stress level of about 85% of the static strength did not cause any failure up to 2×10^6 cycles. Therefore, to conduct the fatigue tests within reasonable amount of time, it was decided to increase the cycling frequency to 10 Hz. The fatigue load ratio used was 0.1 and the specimen were tested at different stress levels ranging from about 54% to 86% of ultimate strength, observed in the quasi-static tests. The cyclic load and displacement data were recorded at a frequency of 100 Hz and tests were conducted till 2×10^6 cycles. If the specimen does not fail in 2×10^6 cycles, the test was stopped and it was considered a runout. The fatigue tests were conducted at 0º, 90º and 45º loading angles; these tests represent uniaxial tensile, pure shear and a biaxial loading condition of equal tensile and shear stresses.

4.3 Fatigue Test Results

The quasi-static test data presented in Chapters 2 and 3 have shown that sheet molding compounds with randomly oriented discontinuous fibers can exhibit large scatter in their strength values as shown in Table 4.1, the fatigue test data also shows large scatter in the life expectancy of the material at different load levels. The stress level in table indicates the maximum stress of the fatigue test as a percentage value of the mean static strength of the specimen.

Initial tests were conducted with stress intervals of 40 MPa starting at 100 MPa. The first specimen failed was at 220 MPa at 97,800 cycles. Additional tests at this stress level indicated that the stress was too high as the specimen failed before the load levels were stabilized. Therefore, the next series of tests were conducted at 200 MPa. These tests showed a large variation in life, which ranged from a failure at 1,714 cycles to runout beyond 2 million cycles. Other tests were conducted at 180 MPa and 190 MPa. Tests at 180 MPa recorded no failure, while the tests at 190 MPa showed a variation in fatigue life.

The tests conducted under shear and 45º biaxial loads were under a maximum cyclic stress level of 100 MPa and 80 MPa. Five specimens were tested at each load level due to time limitation. The fatigue test data for these specimens are given in Table 4.2 and 4.3.

Table 4.1: Tensile fatigue data.

Specimen No.	Area (mm²)	Stress Level (%)	Max Stress (MPa)	Status at 2 million cycles	Life (cycles)
CF-F-013	73.5216	39.0	100	No Failure	-
CF-F-014	73.584	54.6	140	No Failure	-
CF-F-015	72.54	70.2	180	No Failure	-
CF-F-036	72.5712	70.2	180	No Failure	-
CF-F-037	71.9352	70.2	180	No Failure	-
CF-F-038	73.8176	70.2	180	No Failure	-
CF-F-039	72.4319	74.1	190	Failure	340800
CF-F-040	72.3697	74.1	190	No Failure	-
CF-F-041	72.7852	74.1	190	No Failure	-
CF-F-042	71.7332	74.1	190	No Failure	-
CF-F-043	72.1515	74.1	190	Failure	945
CF-F-044	71.3745	74.1	190	No Failure	-
CF-F-019	74.382	78.0	200	Failure	21700
CF-F-020	73.728	78.0	200	No Failure	-
CF-F-021	71.4099	78.0	200	Failure	257100
CF-F-022	71.579	78.0	200	Failure	2558
CF-F-023	72.5874	78.0	200	Failure	1739000
CF-F-025	71.5176	78.0	200	No Failure	-
CF-F-026	72.152	78.0	200	Failure	39650
CF-F-027	71.1172	78.0	200	No Failure	-
CF-F-028	71.248	78.0	200	Failure	1714
CF-F-033	74.2212	78.0	200	Failure	14844
CF-F-034	72.54	78.0	200	Failure	57600
CF-F-035	73.7544	78.0	200	No Failure	-
CF-F-016	72.4712	85.8	220	Failure	97800
CF-F-017	75.5668	85.8	220	Failure	3
CF-F-018	73.458	85.8	220	Failure	4

Table 4.2: Shear fatigue data.

Specimen No.	Area (mm²)	Stress Level (%)	Max Stress (MPa)	Status at 2 million cycles	Life (cycles)
CF-90F-01	71.0398	55.6	80	Failure	406600
CF-90F-02	72.696	55.6	80	No Failure	-
CF-90F-03	70.9308	55.6	80	No Failure	-
CF-90F-04	73.7415	55.6	80	No Failure	-
CF-90F-05	72.2442	69.5	100	Failure	63503
CF-90F-06	71.8734	69.5	100	No Failure	-
CF-90F-07	72.7412	69.5	100	Failure	25550
CF-90F-08	72.0279	69.5	100	No Failure	-
CF-90F-09	72.2142	69.5	100	No Failure	-
CF-90F-10	73.005	55.6	80	No Failure	-

Table 4.3: 45º biaxial fatigue data.

Specimen No.	Stress Level (%)	Max Stress (MPa)	Status at 2 million cycles	Life (cycles)
CF-90F-01	82.5	100	Failure	552673
CF-90F-02	82.5	100	Failure	108138
CF-90F-03	82.5	100	No Failure	-
CF-90F-04	82.5	100	Failure	281800
CF-90F-05	82.5	100	Failure	1359000
CF-90F-06	66	80	No Failure	-
CF-90F-07	66	80	No Failure	-
CF-90F-08	66	80	No Failure	-
CF-90F-09	66	80	No Failure	-
CF-90F-10	66	80	No Failure	-
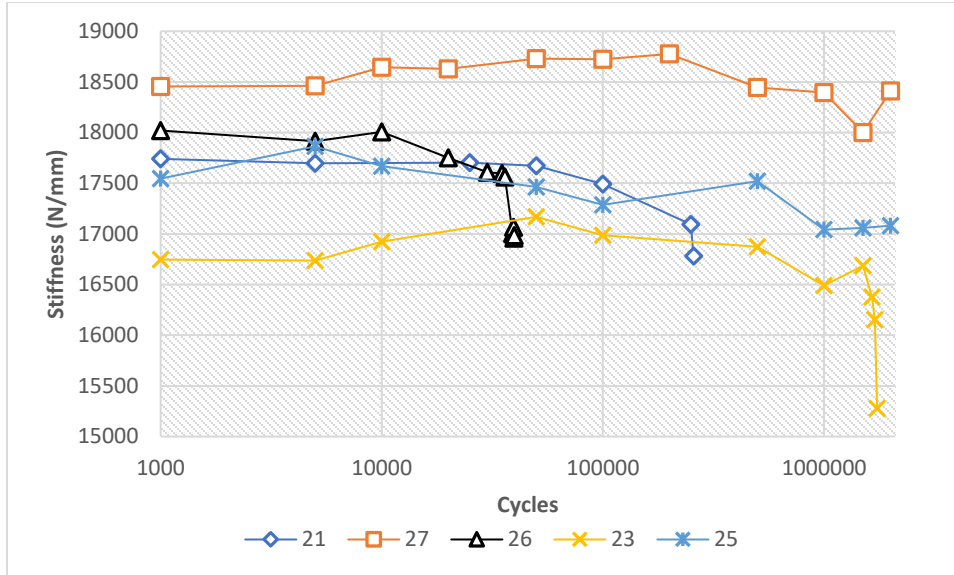
Figure 4.1: Stiffness variation during tensile fatigue test at 78% of the mean tensile strength.

Figure 4.1 shows the change in stiffness during the tensile fatigue tests conducted at a maximum cyclic stress of 200 MPa, which is 78% of the mean tensile strength of the material. The stiffness values of five specimens are plotted in the figure. The stiffness is seen to decrease very gradually with increase in number of cycles in general. Specimen numbers 21, 23 and 26 which failed in fatigue show a drastic decrease in stiffness prior to failure. Specimen numbers 25 and 27 which did not fail in 2×10^6 cycles only show a gradual decrease in stiffness. Also, a variation in the stiffness values is observed from specimen to specimen, which can be attributed to the variation in the material that was observed in the tension tests.

4.4 Statistical Analysis of Fatigue Data

Because of the large variation in fatigue data observed, a statistical analysis of the fatigue test data is performed, which is then used to predict the cyclic life of the material. In this case, since the exact failure time of runout specimens is unknown, the data is right- censored, and standard maximum likelihood methods are used to obtain the best fit for the data. The probability function [30] for right-censored data is given by

$$L(\theta, X) = \prod_{i=1}^{n} f(x_i; \theta)^{\delta_i} \left[1 - F(x_i; \theta)\right]^{1-\delta_i}$$

<div align="right">(4.1)</div>

In equation 4.1, x_i represents failure times, θ represents the distributions parameters, f is the probability density function, and δ_i is the censor variable, which has a value of 0 if the failure time is not censored and 1 if the time is censored. MINITAB is used to conduct the statistical analysis and plot the distribution curves for the test data.

Due to the range of life expectancy of the material at each stress level, the S-N curve is obtained by conducting a statistical analysis of the test data. Weibull, lognormal, and exponential distributions were used to fit curves to the right censored data. The data was right censored at 2 million cycles. Anderson-Darling test was used to find the best fit curve. Figures 4.2 (a) and 4.2 (b) plot the Weibull and lognormal distribution curves for the test data at 0, 45 and 90° loading angles.
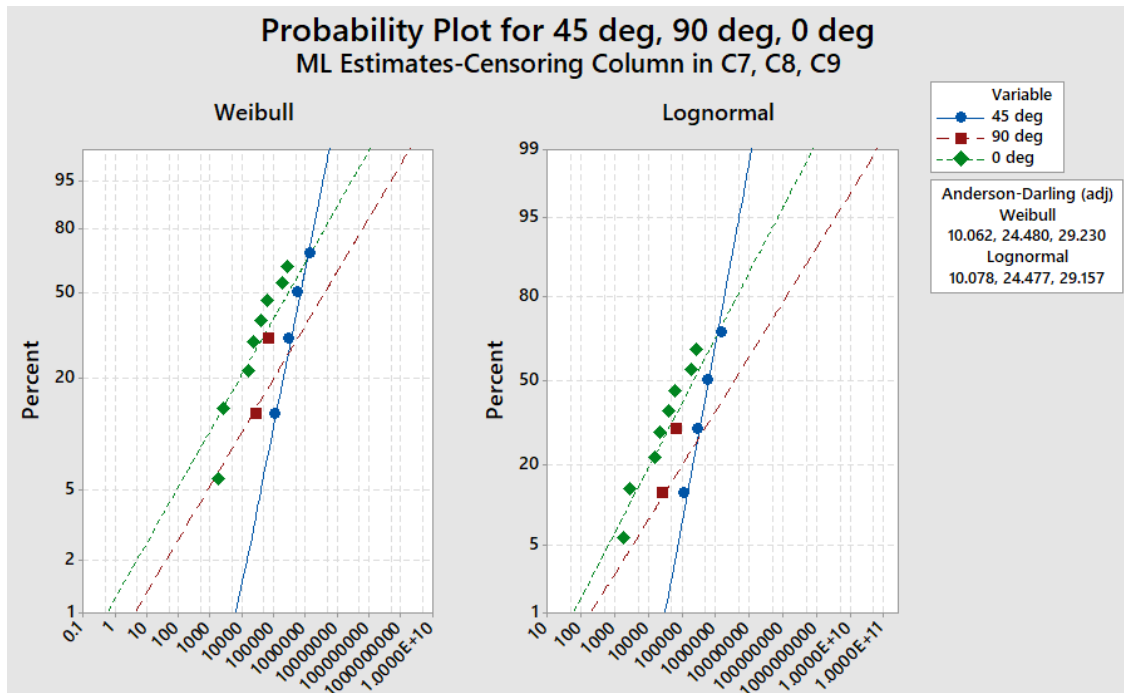
(a)   (b)

Figure 4.2: (a) Weibull and (b) log-normal probability plots for test data at 0, 45 and 90° loading angles at 200 MPa, 100 MPa and 100 MPa, respectively.

The 0° data is at maximum stress of 200 MPa and the 45° and 90° tests are at a maximum stress of 100 MPa. The probability plot indicates percentage of failure on the y-axis and cycles to failure on the x-axis. The best distribution fit for the data is obtained using Anderson-Darling method are shown in the graph. The best fit is different for each case. A similar probability plot comparing Weibull and lognormal distribution for the test data at each fatigue load case is obtained.

Since, there is no distinct life for the specimen at each load level, the S-N curve for the material under tensile fatigue is drawn considering the probability of failure. The data points for the S-N curves are obtained from the probability distribution curves drawn at each loading case. Figure 4.4 shows the S-N curve for the material at three loading directions, tensile, shear and biaxial.

A typical S-N curve represents a relationship between the maximum fatigue stress and the life at that stress level. However, due to the variation in data being observed a simple S-N curve is not sufficient to represent the failure envelope for the material. Hence, the S-N curves presented here represents the life of a specimen at a particular stress level and probability of failure. The curves in Figure 4.3 are drawn at probability of failure equal to 10%. The curves show that the fatigue strength of the material is significant lower under both 45° biaxial load and shear load. The fatigue strength of the material under 45° biaxial load is similar to the fatigue strength under shear load.
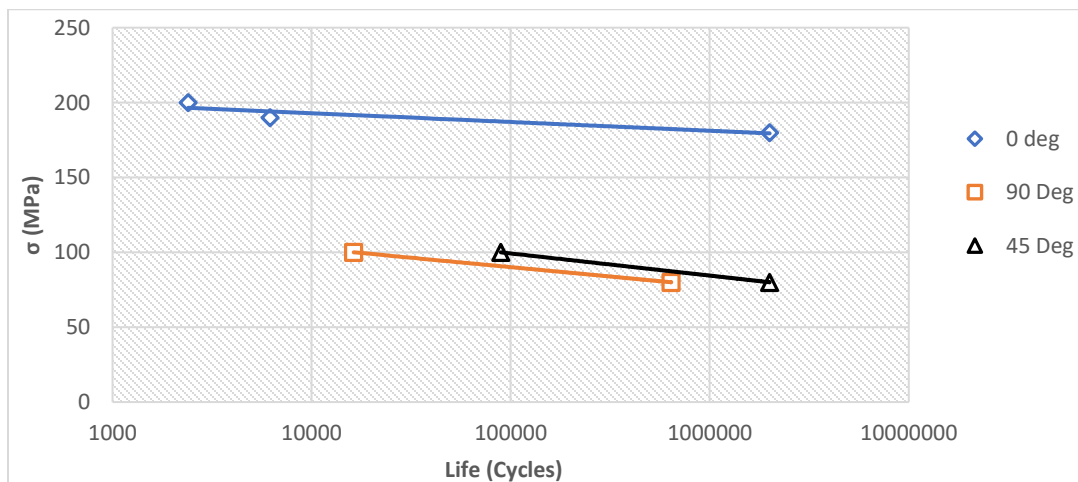
Figure 4.3: S-N curves for carbon fiber SMC-R.
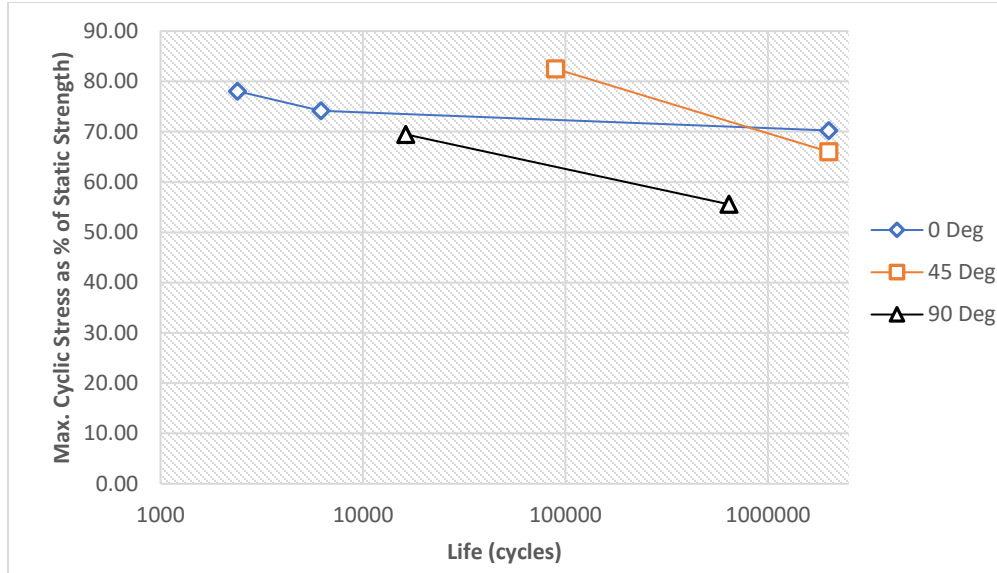
Figure 4.4: S-N curves with maximum cyclic stress represented as percentage of the static strength.

Figure 4.4 shows the S-N curves for carbon fiber SMC-R at tensile, 45° biaxial and shear loading directions. In this figure, the maximum cyclic stress is shown as a percentage value of the static strength of the material in the respective loading angle. It is observed that the fatigue strengths of the material, as a fraction of the static strength, are comparable in tensile fatigue (0° loading angle) and 45° biaxial fatigue. However, under shear fatigue (90° loading angle), it is lower.

4.5 Conclusions

1. Carbon fiber SMC-R was subjected to cyclic tensile, shear and 45° biaxial loads. The material is observed to have a large variation in fatigue life.

2. Standard maximum likelihood methods were used to estimate the life of the material at each stress level due to a large variation in the test results.

3. The fatigue strength of the material shows a significant drop under 45° biaxial stresses and shear stress.

4. The S-N curves for the material are drawn as a function of probability of failure, since there is no distinct life at each stress level. The fatigue strength of the material in 45° biaxial fatigue and shear fatigue are considerably lower than the tensile fatigue.

CHAPTER 5

CONCLUSIONS

5.1 Conclusions

Strength and failure characteristics of SMC-R composites have been studied under different biaxial load conditions using the modified Arcan test method. Glass fiber and carbon fiber SMC-R were used to understand the behavior of these materials under biaxial loading. Glass fiber SMC-R was tested quasi-statically and the carbon fiber SMC-R was subject to both quasi-static and cyclic biaxial loads.

Glass fiber SMC-R was tested at 15° intervals from 0° to 90° to represent tensile, shear and five different biaxial loads. The material is seen to show a significant decrease in strength with the introduction of combined tensile and shear loads. The strength of the material is seen to plateau when shear stress forms a significant portion of the biaxial stress. There is a transition in the load displacement behavior from linear to non-linear due to damage development. This point of transitions is the knee stress, and the non-linearity increases with increase in ratio of shear stress. Failure prediction models were not a good fit for the principal stresses at the peak loads; however, von Mises failure criterion is seen to be a reasonably good fit for the principal stresses at knee load.

Quasi-static biaxial tests were also conducted using carbon fiber SMC-R. This material showed a similar behavior in damage development, and strength under biaxial loading. The material is observed to be planar isotropic in general, but exhibits a large scatter in the properties, especially in the tensile and 45° biaxial specimens. A two parameter Weibull distribution is used to calculate the mean strength of the composite. Hill's failure prediction criterion is observed to closely predict the test data by taking into consideration the through thickness anisotropy of the material.

Finite element analysis was successfully used to understand the stress distribution in the specimen. The crack initiation is seen to originate in a region of tensile and shear stress concentrations, which is slightly away from the significant section of the specimen. Also, the stress distribution across the significant section of the specimen is seen to be mostly uniform over with small variations.

Carbon fiber SMC-R was also tested under cyclic loading to determine their biaxial fatigue behavior. The specimens were tested under tensile, shear and biaxial load conditions. The biaxial loading was done at an angle of 45°. The test data showed a large variation in life of the specimens and hence, statistical analysis was needed to determine the S-N curve of the material. Standard maximum likelihood methods were used to establish the probability of failure at each stress level. The S-N curves obtained for each load condition was a function of the maximum stress, life and the probability of failure. The fatigue strength under shear and biaxial loadings is observed to be significantly lower compared to the tensile fatigue strength.

Comparing the glass fiber and carbon fiber SMC-R, it is observed that the carbon fiber composite shows much higher strength and stiffness in the tensile loading case. Under biaxial loading condition, carbon fiber SMC-R shows a much greater decline in strength and, the stiffness is also observed to be lower. From the load displacement curves for both the materials, the knee point is observed clearly for carbon fiber SMC-R compared to glass fiber SMC-R. This could be due to a higher fiber-matrix bond strength in glass fiber SMC-R. The cracks in both the materials are observed to be similar macroscopically.

Microscopic analysis was conducted using an optical microscope with magnification ranging from 25x to 500x. The images showed failure occurred as a result of fiber matrix debonding and fiber failure in both the materials. In the pure shear loading condition, delamination was also observed in carbon fiber SMC-R.

5.2 Recommendations for Future Work

The findings of this study have shown that sheet molding compounds with discontinuous fibers show a decrease in strength under biaxial load and exhibit variation in properties due to its heterogeneous composition. Further studies should be conducted in the following areas:

- Analysis of defects in the SMC-R sheets prior to testing using NDT methods, to determine the relation between defects and strength of the material.

- Study the microstructure of the damage region.

- Use FEA to find the effect of notch radius on the stress concentration regions near the critical section.

REFERENCES

1. Denton, D. "Mechanical Properties Characterization of an SMC-R50 Composite," SAE Technical Paper 790671, presented at the Passenger Car Meeting, Soc. of Automotive Engineers, June 11-15, 1979.

2. Reigner, D.A. and Sanders, B. A. "A Characterization Study of Automotive Continuous and Random Glass Fiber Composites," presented at the National Technical Conference, Society of Plastics Engineers, November, 1979.

3. Wang, S.S., Chim, E.S.-M., Yu, T.P. and Goetz, D.P. "Fracture of Short-Fiber SMC Composite," *J. Composite Materials*, 1983, vol. 17, pp. 299-311.

4. Wang, S.S. and Chim, E.S.-M. "Fatigue Damage and Degradation in Random Short-Fiber SMC Composite," *J. Composite Materials*, 1983, vol. 17, pp. 114-134.

5. Wang, S.S. and Chim, E.S.-M. and Zahlan, N.M. "Fatigue Crack Propagation in Random Short-Fiber SMC Composite," *J. Composite Materials*, 1983, vol. 17, pp. 250-266.

6. Quaresimin, M. "50th Anniversary Article: Multiaxial Fatigue Testing of Composites: From the Pioneers to the Future Directions," *Strain*, 2015, vol. 51, pp. 16-29.

7. E. W. Smith and K. J. Pascoe. "Biaxial fatigue of a glass–fiber reinforced composite. Part 1: Fatigue and fracture behavior," in *Biaxial and Multiaxial Fatigue (EGF 3)*, M. W. Brown and K. J. Miller, Eds. London: Mechanical Engineering Publications, pp. 367-396, 1989.

8. S. Amijima, T. Fujii, and M. Hamaguchi, "Static and fatigue tests of a woven glass fabric composite under biaxial tension-torsion loading," *Composites*, Jul. 1991, vol. 22, no. 4, pp. 281-289.

9. Mandapati, R. and Mallick, P.K. 2015. "A Study on the Biaxial Fatigue Behavior of E-glass/Epoxy Laminates under Normal and Shear Loadings", presented at the 20th International Conference on Composite Materials, July 19-24, 2015.

10. Arcan, M., Hashin, M. and Voloshin, A. "A Method to Produce Uniform Plane-Stress Sates with Applications to Fiber-Reinforced Materials," *Experimental Mechanics*, 1978, vol. 18, issue 4, pp. 141-146.

11. Douglas L. Denton and Stuart H. Munson-Mcgee, "Use of X-radiographic Tracers to Measure Fiber Orientation in Short Fiber Composites," *ASTM International*, 1985.

12. M. R. Barone and D. A. Caulk "Kinematics of Flow in Sheet Molding Compounds," *Polymer Composites*, April 1985, Vol. 6, No. 2.

13. Alejandro Londono-Hurtado, Tim A. Osswald and Juan Pablo Hernandez-Ortiz "Modelling the Behavior of Fiber Suspensions in the Molding of Polymer Composites," *Journal of Reinforced Plastic & Composites,* 2011.

14. P. K. Mallick, *Fiber-Reinforced Composites,* Third edition, CRC Press, 2008.

15. T. Watanabe and M. Yasuda, "Fracture Behavior of sheet molding compounds. Part 1: Under tensile load", *Composites,* 1982, vol. 13, pp. 54-58.

16. Kai-Youran Hour and Huseyin Sehitoglu, "Damage development in a short fiber reinforced composite," *Journal of Composite Materials,* 1993, Vol. 27.

17. H. Hwang and K. S. Han, "Fatigue of Composites-Fatigue modulus concept and life prediction," *Journal of Composite Materials,* March 1986, Vol 20.

18. Quaresimin, M and Susmel, L. "Multiaxial Fatigue behavior of composite laminates," *Key Engineering Materials,* 2002.

19. A. Smit, D. Van Hemelrijck, T. P. Philippidis, and A. Cardon, "Design of a cruciform specimen for biaxial testing of fiber reinforced composite laminates," *Composites Science and Technology*, Jun. 2006, vol. 66, no. 7-8, pp. 964-975.

20. M. Found, U. Fernando, and K. Miller, "Requirements of a New Multiaxial Fatigue Testing Facility," in *Multiaxial Fatigue*, K. Miller and M. Brown, Eds. 100 Barr Harbor Drive, PO Box C700, West Conshohocken, PA 19428-2959: ASTM International, pp. 11-23.

21. A. Makris, C. Ramault, D. Van Hemelrijck, D. Zarouchas, E. Lamkanfi, and W. Van Paepegem, "An investigation of the mechanical behavior of carbon epoxy cross ply cruciform specimens under biaxial loading," *Polymer Composites*, Sep. 2010, vol. 31, no. 9, pp. 1554-1561.

22. L. V. Smith and S. R. Swanson, "Design of a cylindrical specimen for biaxial testing of composite materials," *Journal of Reinforced Plastics and Composites,* 1997, Vol. 16.

23. Richard B. Freeman, "In-Plane Shear Fatigue Evaluation of SMC," *SAE Technical Papers,* 1987.

24. Hill, R. *The Mathematical Theory of Plasticity*, Clarendon Press, Oxford, 1950.

25. R. Mandapati, "Study of Biaxial Fatigue Behavior of Fiber Reinforced Polymers under Tensile and Fatigue Loadings," Ph.D. Dissertation, Automotive Systems Engineering, University of Michigan-Dearborn, December, 2016.

26. S. C. Hung and K. M. Liechti "Nonlinear Multiaxial Behavior and Failure of fiber-Reinforced Composites," *Time Dependent and Nonlinear Effects in Polymers and Composites, ASTM STP 1357,* 2000, pp. 176-222.

27. Mark Bruderick, Douglas Denton and Michael Shinedling, and Michael Kiesel, "Applications of Carbon Fiber SMC for the Dodge Viper," *Quantum Composites.*

28. Paolo Feraboli, Tyler Cleveland, Marco Ciccu, Patrick Stickler, and Luciano DeOto "Defect and Damage Analysis of Advanced Discontinuous Carbon/Epoxy Composite Materials," *Journal of Composites,* Part-A, 2010, pp. 888-901.

29. Jefri Bale "The Discontinuous Carbon Fiber Composite: A Review of the Damage Characteristics," *LONTAR Jurnal Teknik Mesin Undana, Indonesia,* April 2015, Vol. 2, No. 1.

30. Dustin Dickerson, "Analyzing Right-Censored Data with MLE Techniques," Project Report, *Montana State University,* May 2010.